

Stress rotation — Impact and interaction of rock stiffness and faults

Karsten Reiter

TU Darmstadt, 64287 Darmstadt, Schnittspahnstraße 9

Correspondence: Karsten Reiter (reiter@geo.tu-darmstadt.de)

Abstract. It has been assumed, that the ~~maximum compressive horizontal~~ orientation of the maximum horizontal compressive stress (S_{Hmax}) ~~orientation~~ in the upper crust is governed on a regional scale by the same forces that drive plate motion. However, several regions are identified, where stress orientation deviates from the expected orientation due to plate boundary forces (first order stress sources), or the plate wide pattern. In some of ~~this regions~~ these regions, a gradual rotation of the S_{Hmax} orientation
5 has been observed.

Several second and third order stress sources have been identified in the past, which may explain stress rotation in the upper crust. For example, lateral heterogeneities in the crust, such as density, petrophysical ~~or petrothermal~~ properties and discontinuities, like faults are identified as potential candidates to cause lateral stress rotations. To investigate several of ~~the~~ these candidates, generic geomechanical numerical models are ~~utilized. These models consist of up to~~ set up with up to five
10 different units, oriented by an angle of 60° to the direction of ~~contraction~~ shortening. These units have variable ~~elastic~~ (elastic) material properties, such as Young's modulus, Poisson's ratio and density. ~~Furthermore~~ In addition, the units can be separated by contact surfaces that allow them to slide along these vertical faults, depending on a ~~selected~~ chosen coefficient of friction.

The model results indicate, that a density contrast or the variation of the Poisson's ratio alone ~~sparsely~~ hardly rotates the horizontal stress orientation ($\leq 17^\circ$). Conversely, a contrast of the Young's modulus allows significant stress rotations in the
15 order of up to 78° ; not only ~~areas in the vicinity of the material transition regions near the material transition~~ (<10 km) are affected by ~~that~~ this stress rotation. Stress rotation clearly decreases for the same stiffness contrast, when the units are separated by low friction discontinuities (only 19° in contrast to 78°). Low friction discontinuities in homogeneous models do not change the stress pattern at all ~~away from the fault~~ (>10 km); the stress pattern is nearly identical to a model without any active faults. This indicates that material contrasts are capable of producing significant stress rotation for larger areas in the crust. Active
20 faults that ~~separates~~ separate such material contrasts have the opposite effect, they ~~rather compensate~~ tend to compensate for stress rotations.

Copyright statement. CC BY 4.0

1 Introduction

~~The knowledge growth of the in-situ stress tensor~~ Knowledge of the stress tensor state in the Earth's ~~crust is an important topic~~
 25 upper crust is important for a better understanding of the ~~endogenic dynamic, seismic hazards~~ endogenous dynamics, seismic hazard or the exploitation of the underground. Therefore, several methods have been developed to estimate ~~both, the stress orientation or the stress magnitude~~ the stress tensor orientation and the stress magnitudes. Stress orientation data are compiled globally in the World Stress Map database (Heidbach et al., 2010, 2018; Sperner et al., 2003; Zoback et al., 1989; Zoback, 1992) (Zoback et al., 1992). Based on such data compilations, it was assumed, that patterns of stress orientation on a regional scale are more or less
 30 consistent/uniform within tectonic plates (Coblentz and Richardson, 1995; Klein and Barr, 1986; Müller et al., 1992; Richardson et al., 1997). The plate-wide pattern is overprinted on a regional scale by the ~~current~~ contemporary collisional systems. Recent examples in Europe are the Alps (Reinecker et al., 2010), the Apennines (Pierdominici and Heidbach, 2012) or the Carpathian Mountains (Bada et al., 1998; Müller et al., 2010). Closely related to that ~~are inhomogeneities~~ the variability of crustal thickness, density and topography (Artyushkov, 1973; Ghosh et al., 2009; Humphreys and Coblentz, 2007; Naliboff et al., 2012) (Artyushkov, 1973; Humphreys and Coblentz, 2007).
 35 It was suggested, ~~that remnant stresses due to old plate tectonic events are able to overprint stress orientation on a regional scale~~ (e.g. Eisbacher and Bielenstein, 1971; Richardson et al., 1979; Tullis, 1977) (e.g. Eisbacher and Bielenstein, 1971; Tullis, 1977; Richardson et al., 1979). Such old basement structures also ~~provide~~ present geomechanical inhomogeneities and discontinuities, which have the potential to ~~disturb the stress field~~ perturb the stress pattern. However, pre-Cenozoic orogens (or 'old' suture zones), often covered and hidden by (thick) sediments, ~~and~~ were rarely indicated to cause significant stress rotation. In many cases it is the opposite: old orogens have ~~apparent~~ apparently no impact on the present-day crustal stress pattern, e.g. the Appalachian Mountains (Evans et al., 1989; Plumb and Cox, 1987) (Plumb and Cox, 1987; Evans et al., 1989) or Fennoscandia (Gregersen, 1992). Deviations from the assumed uniform plate-wide stress pattern (here called stress rotations) are observed recently in several regions, such as in Australia, Germany or ~~Northern America~~ (Heidbach et al., 2018; Reiter et al., 2015; Lund Snee and Zoback, 2018, 2020) (Reiter et al., 2015; Heidbach et al., 2018; Lund Snee and Zoback, 2018, 2020). However, these effects can only be
 45 partly explained by the topography or lithospheric structures. ~~Complex~~ The complex stress pattern in central-western Europe was a subject of several numerical investigations in the last decades (Grünthal and Stromeyer, 1986, 1992, 1994; Gölke and Coblentz, 1996; Goes et al., 2000; Marotta et al., 2002; Kaiser et al., 2005; Jarosiński et al., 2006). Apart from a recent 3-D model (Ahlers et al., 2020), the previous models were limited to 2-D. These 2-D models ~~was/were~~ able to reproduce some of the observed stress ~~pattern, applying variable patterns~~ by considering variable lateral elastic material properties or discontinuities. ~~However, the drawback of~~
 50 However, 2-D models ~~are the limitation, that they have~~ have some limitations: They have to integrate topography, crustal thickness and stiffness to one property; ~~furthermore, they overestimate horizontal stresses (Ghosh et al., 2006). None of such studies compared, and they potentially overestimate the horizontal stress magnitude (van Wees et al., 2003; Ghosh et al., 2006).~~ Furthermore, none of these previous studies investigated the impact of the influencing factors separately.
 55 ~~In order to address the question, which properties are able to cause substantial stress rotations away from the material transition or a discontinuity, simple generic models will be used. They are~~ this work, a series of large scale 3-D generic geomechanical models is used to determine which properties can cause significant stress rotations at distance (>10 km) from material transitions or discontinuities. The model geometry is inspired by the crustal structure and the stress pattern in the Ger-

man Central Uplands, where the S_{Hmax} ~~orientations is about 150~~orientation is 120 to 160°. This is in contrast to a ~~north-south~~
60 ~~orientation (N-S orientation (~0°))~~orientation (~0°) of S_{Hmax} to the north and to the south of the uplands (Fig. 1, Reiter et al., 2015). The base-
ment structures there are striking ~~about 30-45 to 60°~~about 45 to 60°, which is almost perpendicular to the observed S_{Hmax} orientation. The
influence of the structures on the stress field will be tested with a generic variation of the Young's modulus, the Poisson's
ratio, the density and vertical low friction discontinuities, which ~~separates~~separate the crustal blocks. Each property is tested
separately first, to avoid interdependencies; possible interactions are tested ~~afterward~~afterwards.

65 2 Stress rotation in the ~~Earth~~upper crust

2.1 ~~Sources~~Concept of ~~crustal stresses~~stress rotation

The major contribution of stresses in crustal Earth is gravity acceleration. The acting body force is a function of density, the
effective gravity and depth. The second major driver are the forces propelling plate tectonics. Plate boundary forces where
identified and derive deviatoric stresses (e.g. ~~????~~Zoback et al., 1989). The visible products of that are collisional zones or
70 orogens, having a significant topography and a crustal root, which are able to overprint crustal stress pattern on a regional scale,
like the fan shape stress pattern in the western and northern foreland of the Alps (Kastrup et al., 2004; Reinecker et al., 2010).
There are several other features in the continental crust, which are also able to bias stress pattern on a local or regional scale.
The most of these features are a product of previous geodynamical processes, such as passive continental margins, sedimentary
~~basins, density~~This study focuses on stress rotations that occur horizontally, i.e. in the map view. A vertically uniform stress
75 field is assumed, which is consistent with previous studies (Zoback et al., 1989; Zoback, 1992; Heidbach et al., 2018). Stress
rotations with depth are occasionally observed within deep wells (Zakharova and Goldberg, 2014; Schoenball and Davatzes, 2017),
due to evaporites (e.g. Roth and Fleckenstein, 2001; Röckel and Lempp, 2003; Cornet and Röckel, 2012), or man-/gravity anomalies,
topography, crustal roots, etc.

A systematic classification was developed to range the manifold stress sources, depending on their spatial coverage in
80 first, second and third order stress sources (~~?~~Heidbach et al., 2010, 2018; Zoback et al., 1989; Zoback, 1992). First order stress
sources extend over a distance of >500 km, which is larger than the thickness of the lithosphere, second order stress sources
extend over a distance of 100–500 km, which is approximate the same thickness like the lithosphere, and third order stress
sources extend over an distance of <100 km, which is smaller than the thickness of the lithosphere. Second and third order stress
sources are able to disturb overall stress orientation trend from regional through local to reservoir scale (~~?~~Heidbach et al., 2010, 2018; ?; Tin

85 First order stress sources next to gravity are plate boundary forces: ridge push, slab pull (~~????~~Zoback et al., 1989; Zoback, 1992),
trench suction (~~?~~), gravitational potential energy (GPE) which is related to the inhomogeneous topography and mass distribution
in the lithosphere (Ghosh et al., 2009; Humphreys and Coblenz, 2007; Naliboff et al., 2012) and basal drag or tractions originating
from mantle convection (Adams and Bell, 1991; ~~??; ??; ??; ??; ?~~).

90 Second order stress sources are lithospheric flexure due to isostatic compensation or sediment loading on continental margins
(Bott and Dean, 1972), membrane stress (~~??~~) seamount loading, upwarping ocean ward of the trench (~~???~~Zoback, 1992),

localized lateral density contrasts/buoyancy forces (Artyushkov, 1973; Bott and Dean, 1972; Fleitout and Froidevaux, 1982), lateral strength contrasts or anisotropy of material properties, topography (?), continental rifting, large fault zones, lateral contrasts of heat production (hydrothermal, volcanic) (?), tensile stress due to cooling of (oceanic) lithosphere (???), flexural stresses due to deglaciation (? Stein et al., 1989; ?) and mass re-distribution on the surface (sedimentation and erosion processes: ???) made activities in the underground (e.g. Martínez-Garzón et al., 2013; Ziegler et al., 2017; Müller et al., 2018).

Third-order stress sources are local density or strength contrasts, internal basin geometry, basal detachments, active faults, remnant stresses as a result of ancient tectonic forces (Eisbacher and Bielenstein, 1971; Richardson et al., 1979; Tullis, 1977) and incised valleys (?). Furthermore, there are man-made increase or decrease of load (e.g. excavations or embankment dams) and downhole pressure changes (production or grouting of fluids).

2.2 The stress tensor

Mechanical stress describes the internal forces in solids that neighbouring particles of a continuous material apply on each other. The stress tensor is a second rank tensor, that consists of nine components from which six are independent on account of the symmetry characteristics. Three of them are normal stresses, orthogonal to each other (σ_{xx} , σ_{yy} , σ_{zz}) and three of them are shear stresses (τ_{xy} , τ_{xz} , τ_{yz}). Choosing an optimal reference system, all shear stresses will disappear ($\tau_{xy} = \tau_{xz} = \tau_{yz} = 0$) and the three normal stresses becomes principal stresses. Such principal stresses are independent from the reference system and are denoted in the order of magnitude: $\sigma_1 > \sigma_2 > \sigma_3$. For areas without topography, having lateral homogeneous material properties and density, such as sedimentary basins, it is assumed, that the vertical stress (S_V) is a principal stress (Anderson, 1951; Brudy et al., 2004). S_V is a cumulative product of the particular rock density, depth and gravity (Herget, 1973). Consequently, both remaining principal stresses are aligned horizontally to the Earth surface, which are the minimum and the maximum horizontal stress (S_{hmin} and S_{Hmax} respectively) and again orthogonal to each other. Using that simplification, the On a map view, several potential sources of stress tensor can superpose on another and the resulting stress at a certain point comprises the sum of all stress sources from plate wide to very local stress sources. Differences between the resulting stress orientation and the regional stress source can be described with the magnitude of S_V , S_{Hmax} and S_{hmin} and the orientation of S_{Hmax} by the angular deviation (Sonder, 1990), which can be substantial and can lead to a change of the stress regime (Sonder, 1990; Zoback, 1992; Jaeger et al., 2007). The stress regime (Anderson, 1905, 1951) are is defined by the relative stress magnitudes, which are normal faulting regime ($S_V > S_{Hmax} > S_{hmin}$; $S_V = \sigma_1$), strike slip regime ($S_{Hmax} > S_V > S_{hmin}$ $S_V = \sigma_2$) and thrust faulting regime ($S_{Hmax} > S_{hmin} > S_V$; $S_V = \sigma_3$).

2.2 Indicators of stress orientation

Data indicating), where S_V is the vertical stress and S_{hmin} and S_{Hmax} orientation in the Earth' crust are compiled since the 1970's (Hast, 1973; Ranalli and Chandler, 1975; ?; ?), using fault plane solutions, overcoring, hydraulic fracturing or geological indicators. After recognition that borehole breakouts can be used as an indicator of S_{Hmax} orientation (????), much more data became available. This led under the International Lithosphere Program to the formation of the World Stress Map (WSM) database. In the first publication, the WSM database comprised 3.574 entries (Zoback et al., 1989) and increased recently to

125 42,870 entries (Heidbach et al., 2018). The WSM database provide an assignment of qualities of the S_{Hmax} orientation data. The quality criteria range from A to E, where A-quality are the most reliable data, and E-quality contain ambiguous or poorly usable information.

There are three large groups of stress indicators, which are derived from different depth ranges. They are geophysical data (<40 km), borehole data ($<<10$ km) and geological data from the Earth surface. The database comprises present-day
130 S_{Hmax} orientation data, derived from single fault plane solutions (FMS), average fault plane solutions (FMA) stress inversion based on fault plane solutions (FMF), borehole breakout data (BO, BOT, BOC), hydraulic fracturing (HF, HFG, HFM, HFP), drilling induced tensile fractures (DIF), overcoring (OC) and geological indicators (volcanic alignment — GVA and fault slip analysis — GFI) and other rare methods. There are many text books and publications available to delve deeply into the methods (Richardson et al., 1979; ?; ?; Zoback, 1992).

135 2.2 Stress rotation in the upper crust

The term stress rotation is used to describe the S_{Hmax} re-orientation vertically (down-well) or rather horizontally i.e. in the map view perspective. The latter is clearly the focus of this study. All the stress sources interact with each other and therefore stress at a certain point comprises the sum of all stress sources from plate wide to very local stress sources. In the case that a regional stress pattern is disturbed by a local stress source, are the minimum- and the maximum horizontal stress, respectively.
140 The difference between the largest and smallest principal stress is the differential stress ($\sigma_D = \sigma_1 - \sigma_3$), while the deviatoric stress is the difference between the resulting stress orientation and the regional stress source can be described by the angle γ (Sonder, 1990). The resulting (counter)-clockwise rotation (γ) can be substantial and can last in a change of the stress regime (Jaeger et al., 2007; Sonder, 1990; Zoback, 1992). state and the mean stress ($\delta\sigma_{ij} = \sigma_{ij} - \sigma_m$, Engelder, 1994)

Shallow stress orientations are mostly consistent with those data, inferred from deep focal mechanism, and therefore a
145 vertical uniform stress field in the brittle crust is assumed (Heidbach et al., 2018; Zoback et al., 1989; Zoback, 1992). However, systematic stress rotations are observed within deep wells (Schoenball and Davatzes, 2017; Zakharova and Goldberg, 2014). This is in particular observed and expected as a result of decoupling by evaporites (e.g. Cornet and Röckel, 2012; Röckel and Lempp, 2003; or man-made activities in the underground (e.g. Martínez-Garzón et al., 2013; Müller et al., 2018; Ziegler et al., 2017). However, both is not a subject of that study. Stress rotation within this study means an angular deviation of the S_{Hmax} orientation from the
150 large-scale stress pattern. In the following subsections, previous observations and models on the respective causes are reviewed and also summarized in Table 1.

Density contrast and topography

2.2 Density contrast and topography

Variability of density within the crust or lithosphere have has a significant impact on the stress state (Artyushkov, 1973; Fleitout and Froidev
155 Assameur and Mareschal (1995) showed, that local stresses stress increase due to topography and crustal inhomogeneities are

Table 1. Comparison of selected previous observations or models on the subject of stress rotation in the context of faults, elastic material properties, density or topography variation. The characters 'X' and 'V' indicate, whether the property is included or varied; '(X)' means, that the subject is included indirectly. The characters '<' and '>' indicate that significant rotation occurs near (<10 km) or at greater distance (>10 km) from the fault or material transition.

Publication	Model (M) or observation (O)	Density / Thickness	max. observed Rotation [°]	Young's moduls	Poisson's ratio	Faults	significant rotation >or <10 km
Grünthal and Stromeyer (1986)	M	-	90	X	X	~	>
Bell and Lloyd (1989)	M	-	~25	V	V	~	>
Bell and McCallum (1990)	O	-	90	-	~	X	<
Sonder (1990)	M	V	90	-	~	~	-
Grünthal and Stromeyer (1992)	M	-	90	V	X	X	>
Grünthal and Stromeyer (1994)	M	-	90	V	X	X	>
Spann et al. (1994)	M	-	90	V	X	~	>
Zhang et al. (1994)	M	-	58	V	V	~	>
Gölke and Coblenz (1996)	M	X	~45	X	X	~	>
Homborg et al. (1997)	M	X	50	X	X	X	<
Mantovani et al. (2000)	M	(X)	90	V	X	V	>
Marotta et al. (2002)	M	X	~35	-	~	~	>
Yale (2003)	O	-	90	-	~	X	<
Jarosiński et al. (2006)	M	(X)	90	V	X	V	>
Mazzotti and Townend (2010)	O	-	50	-	~	X	>

in the order of tens of MPa, which ~~are on the similar magnitude as~~ is on the order of stresses resulting from the plate boundary forces.

Gravitational forces are also derived by surface topography (~~Miller and Dunne, 1996; Zoback, 1992~~)([Zoback, 1992; Miller and Dunne, 1996](#)). On top of mountains, S_{Hmax} is oriented parallel to the ridge and perpendicular at the foot of the mountain chain. Along passive
160 continental margins, similar effects ~~like for topography are to observe~~ ([Bell, 1996; Bott and Dean, 1972; King et al., 2012; Stein et al., 1989](#)) as for topography can be observed ([Bott and Dean, 1972; Stein et al., 1989; Bell, 1996; Yassir and Zerwer, 1997; Tingay et al., 2005; King](#)

Sonder (1990) investigated the interaction of different regional deviatoric stress regimes ($\sigma_D \delta \sigma_{ij}$) with stresses arising from buoyancy forces (σ_G) ~~and observe~~ σ_G and observed a rotation of S_{Hmax} of up to 90°. According to that, S_{Hmax} rotates to-
165 ward the normal trend of the density anomaly. If regional stresses are large, compared to stresses driven by a density anomaly ($\sigma_D/\sigma_G \ll 1 \delta \sigma_{ij}/\sigma_G \gg 1$), the influence of a density anomaly is small and vice versa: If the regional stress is small, ~~compared to the stress driven by the density anomaly~~ ($\sigma_D/\sigma_G \gg 1 \delta \sigma_{ij}/\sigma_G \ll 1$), the impact of a density anomaly on the resulting stress field is large. In the case that both stress sources are on a similar level ($\sigma_D/\sigma_G \approx 1 \delta \sigma_{ij}/\sigma_G \approx 1$), small changes of one

of the stress sources are able to change the stress regime, and ~~therefore potentially the deformation style~~ thus potentially the stress orientation.

Strength-contrast

2.3 Stiffness contrast

Mechanical ~~strength-stiffness~~ describes the material behaviour under the influence of stress and strain. The focus here is on linear elastic material properties, characterized by the Young's modulus and the Poisson's ratio. Stress refraction between two elastic media can be calculated, but only at the interface of the two media, based on the known stress state on one side of the interface and the Young's modulus ~~of both on both sides~~ (Spann et al., 1994). Stress rotation due to ~~strength-contrast are~~ stiffness contrast is e.g. reported for the Peace River Arch in Alberta (~~Adams and Bell, 1991; Bell and Lloyd, 1989; Fordjor et al., 1983; Canada (Fordjor et al., 1983; Bell and Lloyd, 1989; Adams and Bell, 1991)~~). Potential stress rotation is ~~confirmed-supported~~ by several numerical studies (~~Bell and Lloyd, 1989; Grünthal and Stromeyer, 1992; Mantovani et al., 2000; Marotta et al., 2002; Spann et al.,~~

Discontinuities

2.4 Discontinuities

Discontinuities are planar structures within or between rock units, where the shear strength is (~~signifieants~~ significantly) lower than that of the surrounding rock. Genetically, discontinuities can be classified into bedding, schistosity, joints and fault planes. In the context of ~~that this~~ study the term discontinuity refers to fault planes or fault zones. Similar to the Earth surface, (nearly) frictionless faults without cohesion act like a free surface in terms of continuum mechanics (Bell et al., 1992; Bell, 1996; Jaeger et al., 2007). One of the three principal stresses must be oriented perpendicular to the frictionless fault, ~~the~~ the two remaining ones are parallel to the discontinuity. For this reason, the stress tensor ~~bends~~ rotates near a frictionless fault, depending on its orientation. Significant stress rotation in the context of faults ~~are reported (Adams and Bell, 1991; Bell and McCallum, 1990; Mazzotti and Townend,~~ reported (Bell and McCallum, 1990; Adams and Bell, 1991; Yale, 2003; Mazzotti and Townend, 2010). However, Yale (2003) assumes, that stress rotation occurs ~~several kilometres away only within several kilometres~~ from the fault. ~~Small differences between the horizontal stresses increases the effect of faults on the local stress pattern, whereas large stress differences lead to more homogeneous~~ Large differential stress lead to a more stable stress pattern (Laubach et al., 1992; Yale, 2003), ~~whereas low differential stresses allow a switch of the stress regime caused by faults~~. The impact of faults on stress rotation ~~is investigated~~ has been investigated analytically (Saucier et al., 1992) and by numerical models (~~e.g. Homberg et al., 1997; Zhang et al., 1994; Tommasi et~~

3.1 Stress Orientation in Central Europe

Crustal stress data from Europe have been collected since the 1960's (e.g. Froidevaux et al., 1980; Greiner, 1975; Greiner and Illies, 1977; Illies and Greiner, 1978; later within the framework (e.g. Hast, 1969, 1973, 1974; Greiner, 1975; Ranalli and Chandler, 1975; Greiner and Illies, 1977; Froidevaux and Illies, 1978; later as part of the World Stress Map database). These data were applied to investigate the crustal stress pattern for Western Europe (Gölke and Coblentz, 1996; Klein and Barr, 1986; Müller et al., 1992), Scandinavia (Gregersen, 1992), Central Europe (Grünthal and Stromeyer, 1986, 1992, 1994), the Alps (Kastrup et al., 2004; Reinecker et al., 2010), or for the Mediterranean area (?). As principal S_{Hmax} orientation are identified as north-west to north-north-west in Western Europe, a slightly rotation to north-east in central Europe, a west-north-west orientation in Scandinavia and a east-west orientation in the Aegean Sea and western Anatolia, from Zoback et al. (1989) to more recently by Heidbach et al. (2018)

S_{Hmax} orientation in western Europe of $145^\circ \pm 26^\circ$ deviates rotates clockwise by about 17° (Müller et al., 1992) to the direction of absolute plate motion from Minster and Jordan (1978). This is in agreement with Zoback et al. (1989) which who obtained a better fit for relative plate motion between Africa and EuropaEurope, than for absolute plate motion. As major reasons for the major causes of the observed stress pattern in western and central Europe are the ridge push of the Mid-Atlantic ridge and the collisional forces along the southern plate margins are identified (Goes et al., 2000; Gölke and Coblentz, 1996; Grünthal and Stromeyer, 1992). A fan like stress pattern has been observed in the western Alps and Jura mountains, where S_{Hmax} in front of the mountain chain is perpendicular to the strike of the orogen. Müller et al. (1992) assumes (Fig. 1). Müller et al. (1992) assume, that these structures only locally overprints-overprint the general stress pattern. However, in the light of the recently available data, it is assumed, that the S_{Hmax} orientation is rather controlled by gravitational potential energy of the alpine topography than by plate boundary forces (Grünthal and Stromeyer, 1992; Reinecker et al., 2010). The explanation of that crustal structure are a cold, dense and slowly subsiding lithospheric root beneath the Alps (?).

Stress-The stress pattern in western and central Europe has been an the subject of several modelling attempts in the last three decades (Grünthal and Stromeyer, 1986, 1992, 1994; Gölke and Coblentz, 1996; Goes et al., 2000; Marotta et al., 2002; Kaiser et al., 2005; Jarosiński et al., 2006). Among other things, it was examined which factors contributes to the observed stress pattern. Investigated was the In particular, these previous studies investigated the impact of a lateral stiffness contrast in the crust (Grünthal and Stromeyer, 1986, 1992, 1994; Jarosiński et al., 2006; Kaiser et al., 2005; Marotta et al., 2002), the elastic thickness of the crust-lithosphere (Jarosiński et al., 2006), the stiffness contrast of the mantle (Goes et al., 2000), a lateral density contrast or topographic effects (Gölke and Coblentz, 1996; Jarosiński et al., 2006), the post-glacial rebound in Scandinavia (Kaiser et al., 2005) and activity on faults (Kaiser et al., 2005; Jarosiński et al., 2006).

Stiffness variation in the lithosphere, e.g the Teisseyre-Tornquist Zone (TTZ) or the Bohemian Massif (BM), has been identified as the major reasons for a potential cause for the observed stress rotation in Central Europe (Goes et al., 2000; Gölke and Coblentz, 1996). One example is the fan shaped stress pattern in the North German Basin (NGB), with a rotation of S_{Hmax} from north-west in the western part to north-east in the eastern part of the basin as a product of the TTZ, which is the boundary between the Phanerozoic Europe (Avalonia) and the much stiffer Precambrian Eastern European Craton (Baltica). However,

Jarosiński et al. (2006) came to the conclusion, that active tectonic zones and topography ~~has~~ have major effects, whereas the stiffness contrast ~~lead~~ leads only to minor effects. ~~Post-glacial rebound does have an effect on the stress pattern in the NGB (Kaiser et al., 2005).~~ Lateral variation of density ~~do~~ does not have a significant impact on the stress pattern (Gölke and Coblenz, 1996), it ~~provides~~ causes only local effects. Finally, ~~small~~ low differential stress allows significant stress rotation (~~Grünthal and Stromeyer, 1992~~) (Sonder, 1990; Grünthal and Stromeyer, 1992).

3.2 Basement structures in Germany

To large parts, Germany consists of Variscan basement units, either exposed or covered by Post-Paleozoic basin sediments. The Variscan orogen is a product of the late-Paleozoic collision of the plates Gondwana and Avalonia (Laurussia) in late Devonian to early Carboniferous time, which lead to closure of the Rheic Ocean (Matte, 1986), and finally the formation of the super-continent Pangea. Despite the fact, that the European ~~Varieides~~ Variscides are well investigated in the last century and decades (e.g. Franke, 2000, 2006; Kroner et al., 2007; Kroner and Romer, 2013), it is for example still a matter of debate, whether several microplates have been amalgamated in-between or not.

Kossmat (1927) published the structural zonation of the European Variscides, which is still widely used (Fig. 1). The parts to the north-west of the Rheic Suture Zone are the Rheno-Hercynian Zone (RHZ) with the sub-unit of the Northern ~~Phyllite~~ Phyllite Zone (NPZ), both with ~~Laurussian~~ Laurussian origin. South-east of the suture zone are the Mid-German Crystalline High (MGCH), the ~~Saxo-Thuringian~~ Saxo-Thuringian Zone (STZ) and the ~~Moldanubian~~ Moldanubian Zone (MZ); all where exclusively part of ~~Gondwana~~ Gondwana, except the MGCH.

The Rheno-Hercynian Zone (RHZ) is exposed in the Rhenish Massif, in the Harz mountains and in the ~~Felehting~~ Felchtung horst. Dominant are Devonian to lower Carboniferous clastic shelf sediments (Franke, 2000; Franke and Dulce, 2017). These low metamorphic slates, sandstones, ~~greywacke~~ greywacke and quartzite are supplemented with continental and oceanic volcanic rocks, reef limestones and a few older gneisses. Further to the north of the RHZ are the sub-variscan ~~foreland~~ foreland deposits, consisting of clastic sediments and coal seams.

The Northern ~~Phyllite~~ Phyllite Zone (NPZ) is uncovered at the southern edge of the low mountain ranges Hunsrück, Taunus and eastern Harz. ~~Petrological~~ Petrologically it is probably the ~~greenschist~~ greenschist facies equivalent (Oncken et al., 1995) of the Rheno-Hercynian shelf sequence (Klügel et al., 1994), consisting of meta-sediments and within-plate ~~metavolcanic~~ metavolcanic rocks (Franke, 2000).

The Mid-German Crystalline High (MGCH) is open in the Palatinate Forest, Odenwald, Spessart, Kyffhäuser, Ruhla ~~Chrystalline~~ Crystalline (~~Thuringian~~ Crystalline (Thuringian Forest) and ~~Flechting~~ Flechting Horst. It has been interpreted previously as magmatic arc of the ~~Saxo-Thuringian~~ Saxo-Thuringian Zone. But Oncken (1997) assumes that the MGCH is composed ~~from both,~~ Saxo-Thuringian of both, Saxo-Thuringian and Rheno-Hercynian rocks. Composition and metamorphic grade ~~varies~~ vary considerably along-strike of the MGCH (Franke, 2000). It consists of late-Paleozoic sediments, meta-sediments, volcanic rocks, ~~granitoides~~ granitoides, gabbros, ~~amphibolite~~ amphibolite and gneisses.

The ~~Saxo-Thuringian~~ Saxo-Thuringian Zone (STZ) is exposed in the ~~Thuingian-Vogtlandian~~ Thuringian-Vogtlandian Slate Mountains, Fichtel Mountains, Ore Mountains, ~~Saxonian~~ Saxonian ~~Granulite~~ Granulite Massif, Elbe Valley Slate Mountains,

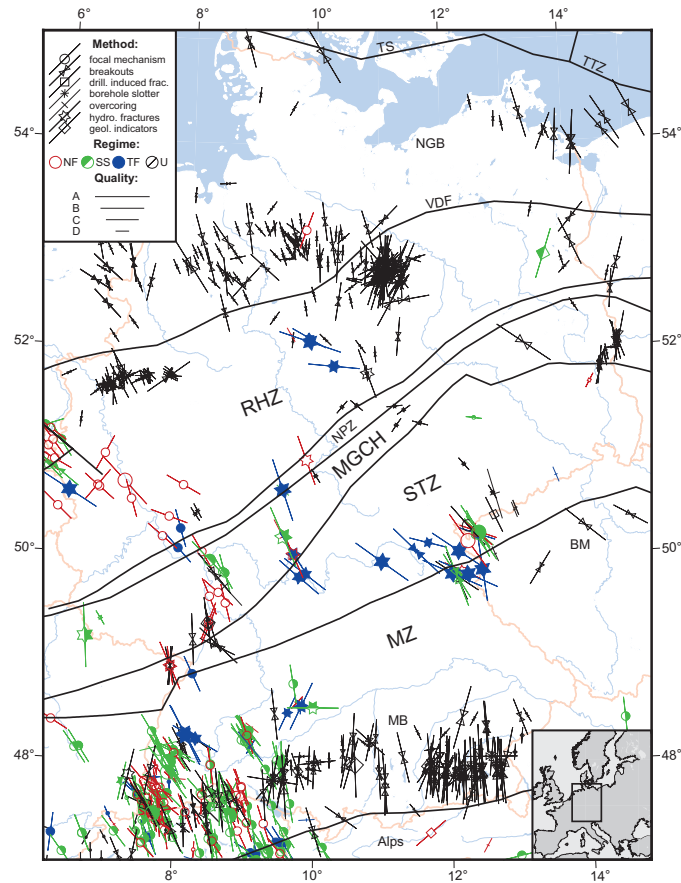


Figure 1. Stress orientation in the German Central Uplands with the basement structural elements (separated by black lines), political boundaries (red) and the major river-rivers (blue). Bars represent orientations-orientation of maximum horizontal compressional stress (S_{Hmax}), line length is proportional to quality. Colours indicate stress regimes, with red for normal faulting (NF), green for strike-slip faulting (SS), blue for thrust faulting (TF), and black for unknown regime (U). The Variscan basement structures, introduced by Kossmat (1927) are visualized; the regional segmentation is: **MZ = Moldanubian Zone**, BM = Bohemian Massif, MGCH = Mid-German Crystalline High, **MZ = Moldanubian Zone**, NPZ = Northern Pyllite Zone, RHZ = Rheno-Hercynian Zone, STZ = Saxo-Thuringian Zone, and VDF = Variscan Deformation Front. Other structures are: **TSMB = Thor Suture**, **TTZ = Teisseyre-Tornquist Zone**, **Molasses Basin**; NGB = North German Basin, **MBTS = Molasses-Basin-Thor Suture**, **TTZ = Teisseyre-Tornquist Zone**. (Redrawn after Franke, 2014; Grad et al., 2016).

and the Lausitz. It consists of Campro-Ordovician mafic and felsic magmatic rocks, late Ordovician to early Carboniferous marine and terrestrial sediments (Franke, 2000; Linnemann, 2004). These rocks underwent metamorphic overprint up to the early Carboniferous with different metamorphism stage up to **eclogite-or-granulite** **eclogite- or granulite** facies. These units are interspersed by late- or post-orogenic granites.

The ~~Moldanubian~~ Moldanubian Zone (MZ) is exposed in the Bohemian Massif, the Bavarian Forest, the ~~Münchberg~~ nchberg Gneiss Massif, the Black Forest and the Vosges. They consist of mostly high grade metamorphic crystalline rocks (gneisses, ~~granulite, migmatite~~ granulite, migmatite) and variscan granites (Franke, 2000).

270 4 Model set-up

4.1 Model ~~dimension~~ geometry

The chosen model geometry is inspired by the geometrical situation in the German Central Uplands (Fig. 1), but the overall intention is a generic model. To make it easy to understand, compass directions are used for model description. The model geometry has a north-south ~~extend~~ extent of 400 km and 300 km in east-west ~~orientation~~ direction, with a thickness of 30 km (Fig. 2).

275 In the centre of the model, three diagonal units ~~having each with~~ a width of 50 km are oriented ~~3060° counter-clockwise from east-west, from north. The unit boundaries are vertically incident. A model variant is generated, in which the unit boundaries allow free sliding, depending on a chosen friction coefficient.~~ For each of the three ~~unit, separate central units, different~~ material properties can be applied. The most northern and southern block has always ~~basie~~ the same (reference) material properties. ~~Furthermore, a model variation is generated, where the units are separated by contact surfaces, allowing free slip depending on a chosen friction coefficient.~~

280 ~~The lateral element resolution is about 3 km consisting primary of hexahedrons and some wedge elements (degenerated hexahedrons). Element resolution into depth ranges from 0.44 km near the surface to about 3.4 km at greatest model depth. The total amount is about 166 k elements; the model version having contact surfaces uses 1725 contact elements along each contact surface. The mesh is generated using HyperMesh® v.2019. The equilibrium of forces (body forces and boundary condition) is estimated numerically using the Abaqus®/Standard v.6.14-1 finite element software.~~

4.2 The Finite Element Method

~~The finite element~~

4.2 Solution of the equilibrium of forces

~~The stress orientations in the models are investigated using the finite element method (FEM) is used since the 1950's to investigate the stability of structures such as wings of an airplane (?). Since the 1970's the method has been introduced in geoscience, to investigate the stress orientation in the Earth crust on certain structures using generic 2-D models (?), or to investigate the stress orientation pattern for large regions (?Grünthal and Stromeyer, 1986). The usage of 3-D FEM models ; to investigate the stress state in the crust is now a well-established technique (e.g. Buchmann and Connolly, 2007; Hergert and Heidbach, 2011). The major reason, that complex 2-D or 3-D models can be computed, is the opportunity to use unstructured meshes.~~

295 The method in general computes the equilibrium of stresses ~~with forces (arising from boundary forces (via displacement boundary conditions) ; and body forces (gravity) and used material properties. Numerically, this is implemented acting on the~~

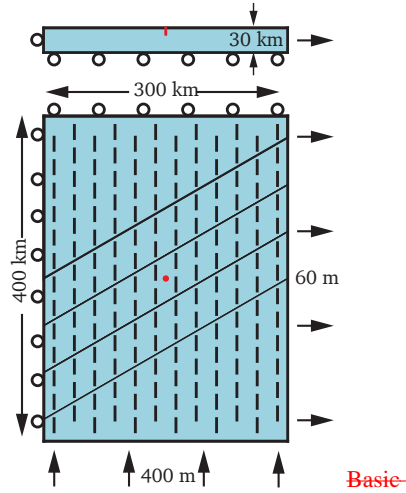


Figure 2. Reference model with the applied boundary conditions, used for all models, in map view and from the south. The model has a lateral extent of 300×400 km and a thickness of 30 km. The model consists of five interconnected units; here visualized in blue, they which have all the basic same material properties (Tab. Blue visualizes the reference material (Table 2). The boundary conditions ban motion in x-direction on the western side, in y-direction on the northern side and in z-direction at the model base. A push of 400 m from the south and a pull of 60 m to the east is applied. The resulting S_{Hmax} orientation (north-south) in at a depth of 1000 m are is illustrated by the black bars. The red point (and line) indicates the location of the virtual well (Fig. 4 and 5). The four diagonal boundaries can be used as discontinuities/vertical faults with a chosen friction coefficient.

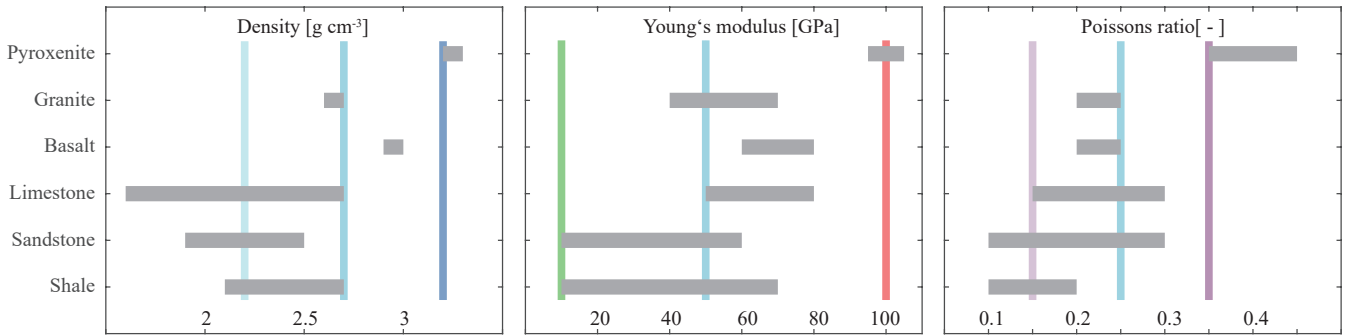


Figure 3. Selection of common elastic rock properties (Young's modulus and Poisson's ratio) and density (Turcotte et al., 2014). Coloured vertical bars indicate applied material properties, see Table 2.

rock whose mechanical behaviour is characterized by a constitutive law and associated material parameters. The equilibrium of forces is represented by partial differential equations:-, which are solved numerically.

$$\frac{\delta\sigma_{ij}}{\delta x_j} \frac{\delta\sigma_{ij}}{\delta x_j} + \rho x_i = 0 \quad (1)$$

300 where $\delta\sigma_{ij}$ is the variation of total stress, δx_j the geometrical-spatial change, and ρx_j represents-represent the weight of the rock section (ρ = density). ~~The previously described balance of forces is well described by the linear elastic material properties (Hooke's law)~~

Linear elastic material behaviour expressed by Hooke's law is assumed. Two material properties, the Young's modulus (E) and the Poisson's ratio (ν) are essential; ~~density is not absolutely necessary but enables that body forces act~~. The stress state in
305 this study will be calculated based on defined displacement boundary conditions ~~-(Fig. 2)~~.

4.3 Material properties

The lateral resolution of the model is about 3 km consisting primary of hexahedrons and some wedge elements (degenerated hexahedrons). Resolution into depth ranges from 0.44 km near the surface to about 3.4 km at the base of the model. In total, about 166.000 elements were used. The model version having contact surfaces uses 1725 contact elements along each contact
310 surface. Model discretization was performed with HyperMesh® v.2019. The equilibrium of forces (body forces and boundary condition) is computed numerically using the Abaqus®/Standard v.6.14-1 finite element software.

4.3 Mechanical properties

The main subject of ~~that~~-this study is to investigate the impact of the variation of elastic rock properties, density and friction along faults on stress orientation in the upper crust ~~-in the given geometrical setting outlined in the previous sections (Fig. 2)~~. To
315 do this, each parameter is tested individually. Figure 3 visualize-visualizes the range of density (ρ), Young's modules-modulus (E) and Poisson's ratio (ν) of representative rocks, taken from a textbook ~~(?)~~(Turcotte et al., 2014).

~~Selection of common elastic rock properties (Young's modulus and Poisson's ratio) and density (?). Coloured vertical bars indicate applied material properties.~~

~~The basic~~-The reference material for this investigation has a density of $\rho = 2.7 \text{ g cm}^{-3}$, a Poisson's ratio of $\nu = 0.25$ and
320 a Young's modulus of $E = 50 \text{ GPa}$. Such a material could represent for example granite or limestone. Based on this basic reference material, always a lower and higher material value is defined (Tab. Table 2), which is within the range of common rocks properties (Fig. 3). The material with a low density ($\rho = 2.2 \text{ g cm}^{-3}$) may represent sediments (sandstone, limestone, shale etc.), ~~where~~-whereas the high density material ($\rho = 3.2 \text{ g cm}^{-3}$) could represent a rock from the lower crust or the upper mantel-mantle. A low Poisson's ratio ($\nu = 0.15$) may represent sediments (sandstone or shale), and a high Poisson's
325 ratio ($\nu = 0.35$) could represent ultramafic rock-rocks. Soft material with a low Young's modulus ($E = 10 \text{ GPa}$) may represent sediments, pre-damaged or weathered rock. Again ultramafic rock is an example for a stiff rock, having a large Young's modulus ($E = 100 \text{ GPa}$).

Laboratory rock experiments in the past delivered friction coefficients of about ~~$\mu = 0.6$ to 0.85~~ - $\mu = 0.6$ to 0.85 (Byerlee, 1978). However, recent investigations using realistic slip rates for earthquakes decreased estimated friction coefficients by one

Table 2. ~~Material properties~~ Young's modulus, Poisson's ratio and densities ~~which has been~~ used in the models. Bold numbers indicate the properties used, which differ from those of the ~~basic reference~~ material.

Name	Young's Modulus [GPa]	Poisson's ratio [-]	Density [g cm ⁻³]
Basic <u>Reference</u> material (B)	50	0.25	2.7
Low Density (g)	50	0.25	2.2
High Density (G)	50	0.25	3.2
Low Poisson (p)	50	0.15	2.7
High Poisson (P)	50	0.35	2.7
Low Stiffness (e)	10	0.25	2.7
High Stiffness (E)	100	0.25	2.7
Upper Mantle	130	0.25	3.25

330 order of magnitude ~~up to $\mu < 0.1$~~ down to $\mu < 0.1$ (Di Toro et al., 2011). Faults are represented by cohesionless contact surfaces in the models. The used friction coefficients are 0.1, 0.2, 0.4, 0.6, 0.8 and 1.0, which ~~finally covers slow~~ covers both, slow and fast slip rates ~~as well~~.

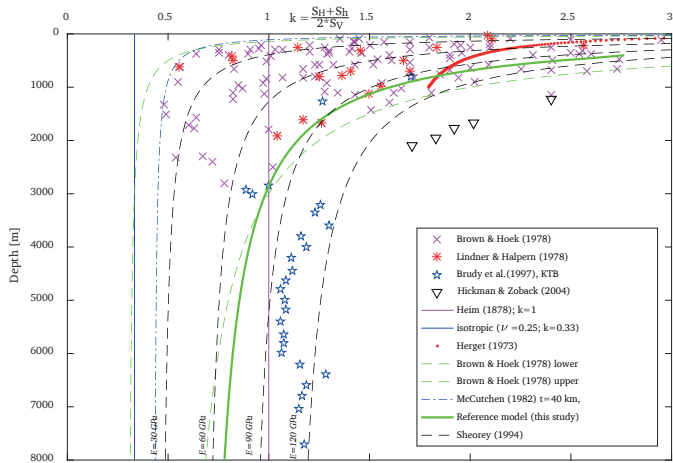


Figure 4. The Stress ratio k (Eq. 2) is plotted versus depth. Stress in the reference model is marked with the bold green line. Additionally, several data and defined stress ratios from the literature are visualized for comparison. (Heim, 1878; Herget, 1973; Brown and Hoek, 1978; Lindner and Halpern, 1978; McCutchen, 1982; Sheorey, 1994; Brudy et al., 1997; Hickman and Zoback, 2004).

4.4 Initial stress state

335 The present day stress state in the crust is a complex product of several stress sources from the past to the present. In order to model the stress state an initial stress state is defined, which is in equilibrium with the body forces (gravity) and which subsequent undergoes lateral straining to account for tectonic stress. Sheorey (1994) provided a simple semi-empirical function (Eq. 2) for the stress ratio k (Eq. 3).

$$k = 0.25 + 7E \left(0.001 + \frac{1}{z} \right) \quad (2)$$

$$k = \frac{S_{Hmean}}{S_V} = \frac{S_{Hmax} + S_{Hmin}}{2S_V}. \quad (3)$$

340 Sheorey's equation (Eq. 2) is a reliable stress ratio versus depth estimation, when compared to real world data (Fig. 4). The model is pre-stressed with zero horizontal strain boundary conditions. The used pre-stressing method has so far been used several times (Buchmann and Connolly, 2007; Hergert and Heidbach, 2011; Reiter and Heidbach, 2014). The model is allowed to compact several times under application of the body forces (gravity) using a Poisson's ratio of $\nu = 0.396$ during that procedure only. During the pre-stressing procedure, models with contact surfaces have a very large friction coefficient ($\mu = 10$) to prevent slip. At a virtual well in the centre of the model ($x=150$ km; $y=200$ km) stress was extracted from the model and compared to the stress magnitude data, which are visualized in Fig. 4 and 5, showing a good fit to stress-depth distribution assumptions (Heim, 1878; Herget, 1973; Brown and Hoek, 1978; McCutchen, 1982; Sheorey, 1994) and measured magnitude ratios as well as (Brown and Hoek, 1978; Lindner and Halpern, 1978; Brudy et al., 1997; Hickman and Zoback, 2004)

4.5 Boundary conditions

350 The overall S_{Hmax} orientation on an imagined profile along longitude 11° (Fig. 1) displays a north-south orientation in the North German Basin (NGB) and in the ~~Molasses~~-Molasse Basin (MB) north of the Alps, except the Variscan basement units in-between. ~~According to that~~ Correspondingly, a north-south orientation of S_{Hmax} is intended for the ~~basie~~-reference model. To ~~define~~-create a meaningful stress state in the model, appropriate boundary conditions (lateral strain) ~~,results are needed. Results~~ from a virtual well in the model centre are compared with data from deep wells. ~~Several strain scenarios where applied to the~~ pre-stressed ~~basie~~ model. An extension of 60 m (~~$\epsilon_x = 0.02$~~ $\epsilon_x = 2 \times 10^{-4}$) in east-west direction and a shortening of 400 m (~~$\epsilon_y = -0.1$~~ $\epsilon_y = -1 \times 10^{-3}$) in north-south direction (Fig. 2) provides a good fit to stress magnitudes from selected deep wells (Fig. 5, Brudy et al., 1997; Hickman and Zoback, 2004; Lund and Zoback, 1999). By fitting the data, the focus was more on the observed S_{Hmin} magnitudes and to ~~a less extend~~ less extent on the S_{Hmax} magnitudes. The latter are less reliable, as they are usually not measured; they are calculated on the basis of several assumptions.

360 4.6 Model scenario's

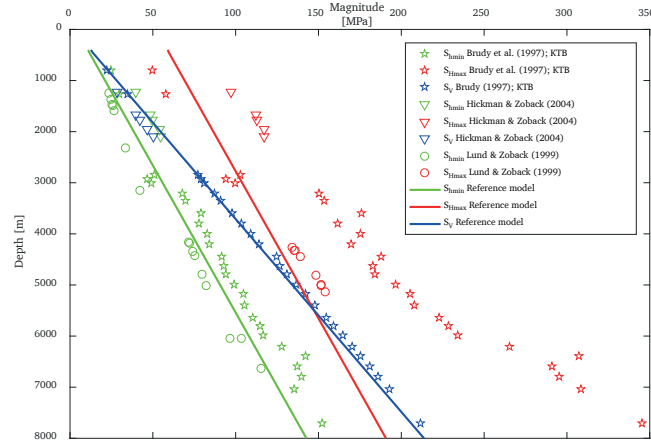


Figure 5. ~~Stress~~The stress magnitudes are ~~potted~~versus ~~plotted~~ as a function of depth. The stress components from the virtual well in the ~~centre of the basic~~model are ~~shown~~illustrated by the ~~coloured~~ lines, ~~using~~. The location of the ~~virtual well and used~~ boundary conditions ~~illustrated~~are shown in Fig. 2. Due to the applied initial stress conditions, the stress regime ~~switches~~changes from thrust faulting ~~in at~~ a depth of ~~around~~400 m ~~below the surface~~to strike slip faulting, and finally to a normal faulting regime ~~in at~~ a depth ~~grater then~~greater than 5500 m. ~~Additionally, published~~Published stress magnitude data are shown for comparison (Brudy et al., 1997; Hickman and Zoback, 2004; Lund and Zoback, 1999)(Brudy et al., 1997; Lund and Zoback, 1999; Hickman and Zoback, 2004).

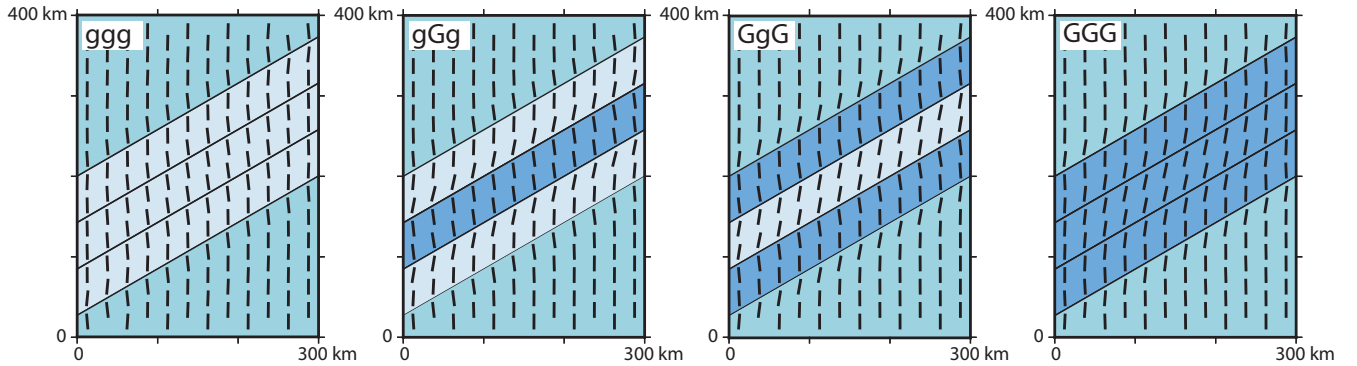


Figure 6. Influence of density on the stress orientation. Black bars represent the orientation of S_{Hmax} at a depth of 1000 m. Colours indicate the used material properties. The medium blue area uses the reference material properties ($\rho = 2.7 \text{ g cm}^{-3}$), the light blue material uses a lower density (g; $\rho = 2.2 \text{ g cm}^{-3}$), the dark blue a larger density (G; $\rho = 3.2 \text{ g cm}^{-3}$).

4.6 Generic model scenario's

The model geometry consists of five units (Fig. 2). The northern- and southern most block ~~uses always the basic~~are always assigned the reference material properties (Tab. Table 2). In between ~~there~~ are three diagonal units, ~~where material properties or friction properties will be varied. The numerical in which material properties are varied.~~ Along the vertical borders within

the model, friction properties can be used. The lower (L) or higher (H) values of the material properties with respect to the reference material properties regarding the basic material (B) will be varied in the following way: LLL, HHH, LBL, BLB, etc. When the model geometry mimics discontinuities using contact surfaces, all contacts have the same friction coefficient. The visualization takes place in the following way, where In the results figures the label 'l' indicates the contact. For example, HLH with four contacts is lHlHlHl.

The S_{Hmax} orientation will be visualized for is visualized at a depth of 1000 m below the surface using a pre-defined pattern grid, where the lateral distance to the material transition or discontinuity is $>>12.5$ km, as far field effects are the major interest of that study.

main interest of this study. The variation of the density, the density, Poisson's ratio, the Young's modulus ,the and friction coefficient will be tested first. Additionally, the Variation In addition, the variation of Young's modulus using is tested in interaction with low friction contacts, a modification of the model with an additional.

Table 3. Material properties used for the scenario using realistic rock properties for to the Variscan basement units; properties are estimated based on Turcotte et al. (2014).

Variscan units	Density ρ [g cm ⁻³]	Young's modulus E [MPa]
Rheno-Hercynian (RHZ)	2.10	20
N. Phyllite (NPZ)	2.20	30 km stiff mantle and a thinner model, having a thickness of only 10 km will be tested. The latter are only n
Mid-German C. (MGCH)	2.75	70
Saxo-Thuringian (STZ)	2.60	50
Moldanubian (MZ)	2.75	70

4.7 Realistic rock property scenario

A reality-based rock property scenario, inspired by the structural zonation of the European Variscides according to Kossmat (1927), is tested. The Rheno-Hercynian Zone (RHZ) and the Northern Phyllite Zone (NPZ) are dominated by clastic shelf sediments with a low- or mid-metamorphic overprint, which are slate (RHZ) and phyllite (NPZ). This zone, the RHZ and the NPZ together, is the most flexible one, and will have the lowest Young's modulus (Table 3). The Mid-German Crystalline High (MGCH) consists of granitoids or gabbros and their metamorphic equivalents (gneiss, amphibolite), meta-sediments and some volcanites. Therefore, this zone is a stiff unit. The Saxo-Thuringian Zone (STZ) is dominated by meta-sediments, mafic and felsic magmatites and their metamorphosed equivalents, and some high-grade metamorphic rocks (granulite, eklogite). Taking all the different rock types into account, the STZ is stiffer as the RHZ and softer than the MGCH. Mechanical, the Moldanubian zone (MZ) can be represented by high-grade metamorphic rocks (gneiss, granulite, migmatite) and granitoids and will be a stiff

unit, similar to the MGCH. Therefore, the unit stiffness are from the deformable to the rigid ones: $RHZ < STZ < MGCH \approx MZ$. Used material properties are estimated based on typical rock values (Table 3). The same initial stress procedure, boundary condition and visualization procedure are applied as previously described.

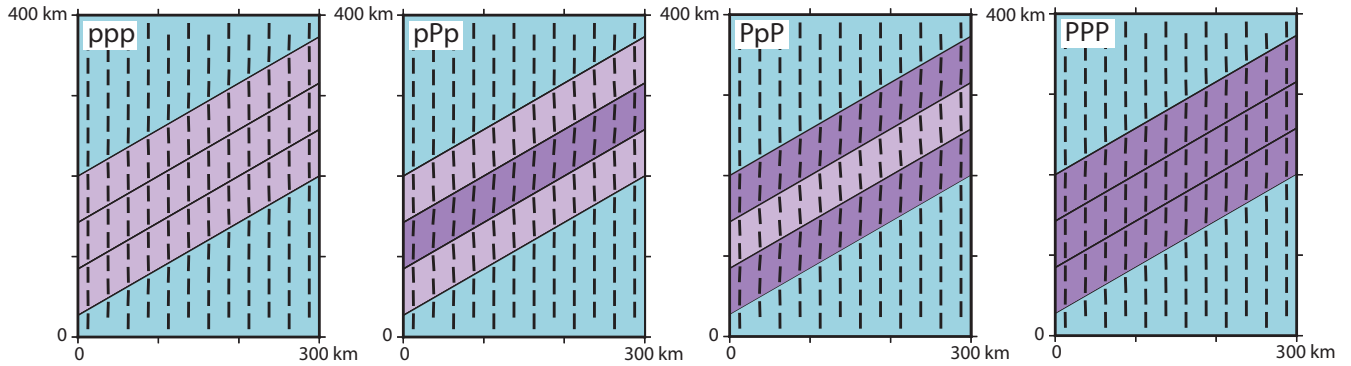


Figure 7. Influence of the Poisson's ratio on the stress orientation. Black bars represent the orientation of S_{Hmax} at a depth of 1000 m. Colours indicate the used material properties. The blue area uses the reference material properties ($\nu = 0.25$), the light purple area is characterized by a low Poisson's ratio (p: $\nu = 0.15$) and the dark purple one by a large Poisson's ratio (P: $\nu = 0.35$).

5 Resulting stress rotation Results

5.1 Density influence

To identify the influence of a density variation, the basic-reference density ($\rho = 2.7 \text{ g cm}^{-3}$) in blue are is varied using a small density (g: $\rho = 2.2 \text{ g cm}^{-3}$), which is coloured in light blue and a large density (G: $\rho = 3.2 \text{ g cm}^{-3}$), which is dark blue in Fig. 6.

Influence of density on the stress orientation. Black bars represents the orientations of the maximum horizontal compressional stress (S_{Hmax}) at a depth of 1000 m. Colours indicate the used material properties. The blue area uses the basic material properties ($\rho = 2.7 \text{ g cm}^{-3}$), the light blue material uses a lower density (g: $\rho = 2.2 \text{ g cm}^{-3}$), the dark blue a larger density (G: $\rho = 3.2 \text{ g cm}^{-3}$).

The low density anomaly (ggg) result in a slightly results in a slight counter-clockwise (-6°) rotation of the S_{Hmax} orientation in the basic-reference material near the anomaly (Fig. 6). Within the low density units near the basic-reference material, nearly no rotation is to observe (-1°), but S_{Hmax} orientation turns more counter-clockwise (-8°) in the centre of the material anomaly. The angular variation of S_{Hmax} crossing the units is in the order of 7° . The high-density anomaly (GGG) results in a slightly clockwise rotation ($+7^\circ$) in the basic-reference material near the anomaly. In the high density unit near the basic-reference material, S_{Hmax} is minimally influenced ($+1^\circ$), but rotates further clockwise ($+12^\circ$) in the centre of the anomaly. Based on that, the variation across the units is about 11° . The models with mixed densities in the three-three units show a clockwise

405 rotation ($+10^\circ$) of S_{Hmax} within the lighter material next to the ~~more-dense~~denser units. The high density units show a counter-clockwise rotation (-7°) next to the low density unit; therefore, the total variation of S_{Hmax} is 17° .

In general, S_{Hmax} ~~is~~tends to be oriented parallel to the anomaly in low density units and perpendicular to the anomaly in the large density units. In the centre of the low density units (ggg), the stress orientation becomes perpendicular to the overall structure. ~~For~~In the centre of the high density units (GGG) ~~happens the opposite~~the opposite is true, S_{Hmax} becomes parallel
410 to the ~~spacious~~ structure.

5.2 Influence of the Poisson's ratio

~~Influence of the Poisson's ratio on the stress orientation. Black bars represents the orientations of the maximum horizontal stress (S_{Hmax}) at a depth of 1000 m. Colours indicate the used material properties. The blue area uses the basic material properties ($\nu = 0.25$), the light purple material uses a low Poisson's ratio (p: $\nu = 0.15$), where the dark purple material have a large Poisson's ratio (P: $\nu = 0.35$).~~
415 ~~Poisson's ratio (P: $\nu = 0.35$).~~

The influence of the Poisson's ratio on the stress rotation is tested by variation of the ~~basie~~reference Poisson's ratio ($\nu = 0.25$) using a lower one (p: $\nu = 0.15$) in light purple and a larger one (P: $\nu = 0.35$) in dark purple .-

in Fig. 7. The models with only a lower (ppp: -1.5°) and only a higher Poisson's ratio (PPP: $+2.2^\circ$) ~~shows~~show only little S_{Hmax} rotation (Fig. 7). Mixed models with largest Poisson's ratio variation (pPp and PpP) have some counter-clockwise
420 rotation in the low Poisson's ratio units (-3.0°) and a clockwise rotation in the high Poisson's ratio units ($+4.2^\circ$). Therefore, the total variance of S_{Hmax} is about 7.5° .

5.3 Impact of Young's modulus

The impact of the Young's modulus ~~variation is investigated taking a basie~~is investigated using the reference material (B: $E = 50$ GPa) in contrast to a softer material (e: $E = 10$ GPa) in green and a stiffer material (E: $E = 100$ GPa) in red(, see Fig. 8).

~~Influence of Young's modulus on the stress orientation. Black bars represent the orientations of the maximum horizontal stress (S_{Hmax}) at a depth of 1000 m. Colours indicate the used Young's modulus; the blue area uses the basic material properties (B: $E = 50$ GPa), the green material uses a low Young's modulus (e: $E = 10$ GPa), where the red material have a large Young's modulus (E: $E = 100$ GPa).~~
425 ~~modulus (E: $E = 100$ GPa).~~

~ The models with the soft units (eee, eBe and BeB) exhibit a strong clockwise S_{Hmax} rotation ($+56^\circ$) in the units with
430 the ~~basie~~reference material and a counter-clockwise rotation in the softer units (-22°) near the material transitions(Fig. 8).

~ Within the models having three soft units (eee) the S_{Hmax} orientation ~~decreases~~decreases to -5° in the centre of the units. ~~That means~~This means that the S_{Hmax} variation within the soft units ~~S_{Hmax} variation~~ is considerable (17°). The resulting total variation is 78° . The models with the stiff units (EEE, EBE and BEB) ~~exhibits~~exhibit a gentle counter-clockwise rotation in the units with the ~~basie~~reference material (-5.5° to -7°) next to the stiff units. Within the stiff units, a significant clockwise
435 rotation ($+20^\circ$ to $+25^\circ$) is apparent next to the ~~basie~~units. The reference units. In the model having three stiff units (EEE), the S_{Hmax} orientation ~~decreases~~decreases to ($+5^\circ$) in the centre. This is a considerable S_{Hmax} variation of ~~considerable~~ 15° within the stiff units. The total variation is 31° .

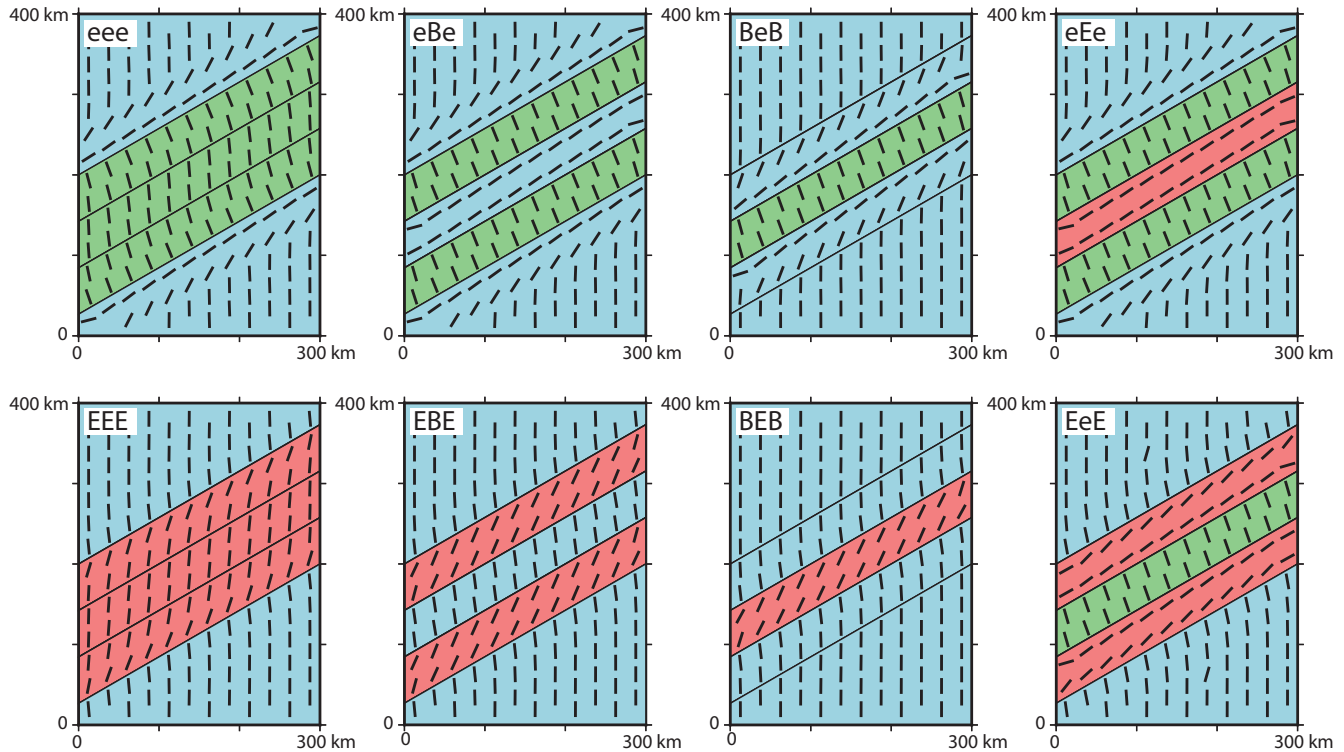


Figure 8. Influence of Young's modulus variation on the stress orientation. Black bars represent the orientation of S_{Hmax} at a depth of 1000 m. Colours indicate the used Young's modulus; the blue area uses the reference material properties (B: $E = 50$ GPa), the green material uses a low Young's modulus (e: $E = 10$ GPa) and the red material has a large Young's modulus (E: $E = 100$ GPa).

For the models with alternating ~~units with~~ soft and stiff material ~~units~~ (EeE and eEe), the soft units ~~exhibits~~ ~~exhibit~~ a counter-clockwise S_{Hmax} rotation (-19° to -22°), ~~where~~ ~~whereas~~ the stiff units ~~displays~~ ~~display~~ a clockwise rotation ($+53^\circ$ to $+56^\circ$).
 440 Consequently, the total variation between the soft and stiff units is 72° to 78° . The general observation is, that next to the material transition, S_{Hmax} rotates perpendicular to the anomaly for the ~~weak~~ ~~compliant~~ units and parallel for the stiff units.

5.4 Influence of faults

Several models with the ~~basie~~ ~~reference~~ material properties separated by three discontinuities (IBIBI) having a friction coefficient (μ) from 0.1 to 1 are tested. The low friction coefficient ($\mu = 0.1$) leads to a counter-clockwise S_{Hmax} rotation of only -3° (Fig. 9). ~~The maximum observed fault offset is about 16 m.~~ By increasing the friction coefficient to $\mu = 0.2$, the S_{Hmax} rotation is -2° , for $\mu = 0.4$, S_{Hmax} rotation is ~~only~~ -1° . For larger friction coefficients, the S_{Hmax} rotation is below -1° . As the S_{Hmax} rotation is too small for a visual differentiation, only the $\mu = 0.1$ model is shown in Figure 9.

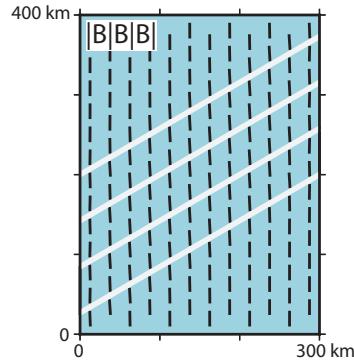


Figure 9. Influence of low friction faults on the far field stress orientation. Black bars ~~represents~~ represent the orientation of ~~the maximum horizontal compressional stress~~ (S_{Hmax}) at a depth of 1000 m. All areas have the ~~basic material~~ properties of the reference material (Tab. Table 2:). White lines indicate ~~cohesionless~~ cohesionless discontinuities (vertical faults). The model using a friction coefficient of $\mu = 0.1$ along the three discontinuities is shown. The other models with a larger friction coefficient (up to 1 and larger) have similar results, they are waived out because of the visual similarity.

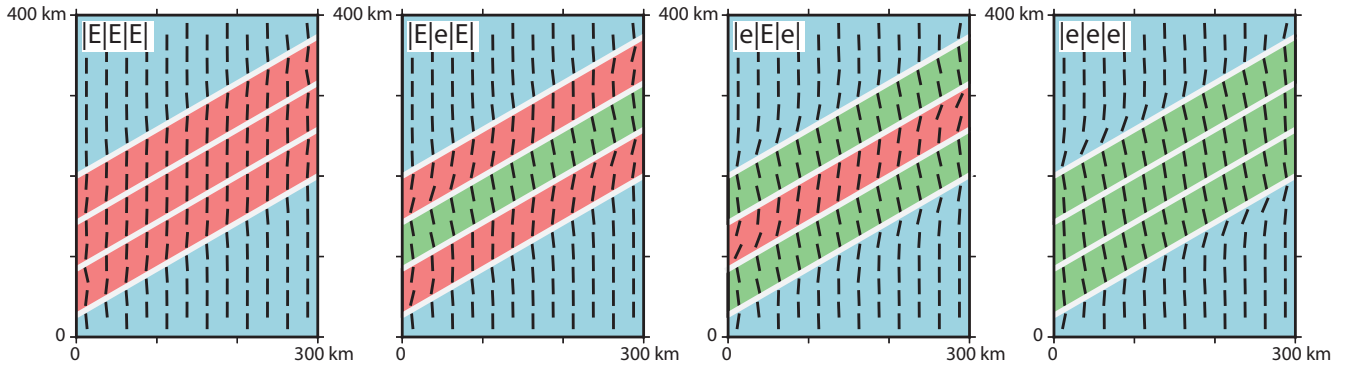


Figure 10. Influence of Young's modulus in interaction with low friction faults on the far field stress orientation. Black bars represent the orientation of S_{Hmax} at a depth of 1000 m. Colours indicate the used material properties. The blue area uses the reference material properties, the green material uses a low Young's modulus and the red material has a larger Young's modulus, see Table 2. White lines indicate cohesionless vertical discontinuities (faults) with a friction coefficient of $\mu = 0.1$.

5.5 Stiffness variation combined with low friction faults

The interaction of a significant Young's modulus ~~difference is tested in combination with a contrast with a cohesionless contact~~ with a low friction coefficient ($\mu = 0.1$) is tested along all four discontinuities. The model with three stiff units (E|E|E) provides only little counter-clockwise rotation (-4°) in the ~~basic~~ reference material near the material transition (Fig. 10). Similar clockwise rotation ~~occur~~ occurs in the stiff units ($+4^\circ$) near the material transition ~~, which and~~ decreases to the material centre centre of the units ($+1^\circ$). ~~However, the~~ The total S_{Hmax} variation ~~of is~~ is about 8° .

Influence of Young's modulus in interaction with low friction faults on the far field stress orientation. Black bars represents the orientations of the maximum horizontal stress (S_{Hmax}) at a depth of 1000 m. Colours indicate the used material properties. The blue area uses the basic material properties, the green material uses a low Young's modulus, where the red material has a larger Young's modulus, see Tab. 2. White lines indicate cohesionless discontinuities (faults) with a friction coefficient of $\mu=0.1$.

The model with the soft units and the low friction discontinuities (lelelel) displays point out significant larger rotation than for the stiff units. Clockwise rotation of $+19^\circ$ occurs in the basic-reference material and counter-clockwise rotation of -13° in the soft units. This decreases toward towards the centre of the soft units (-9°). Both rotations together result in Overall rotation is about 32° .

In the models with the alternating stiffness with the low friction discontinuities (lElElEl and lElElEl) provides-generate a counter-clockwise rotation of about -10° to -12° in the soft units. Within the stiff units, the S_{Hmax} orientation is in the range of $+2^\circ$ to $+7^\circ$. The total variation is up to 19° . The maximum observed fault offset is about 10 to 15 m.

5.6 Stress rotation for realistic material properties

The resulting S_{Hmax} orientation (Fig. 11 a) of the model using realistic material properties (Table 3) indicates counter-clockwise rotation in the RHZ (Rhenio-Hercynian Zone) and NPZ (Northern Phyllite Zone) and clockwise rotation within the MGCH (Mid-German Crystalline High) and MZ (Moldanubian Zone) units. The overall pattern of the simple model (Fig. 11 a) shows only limited similarity with the observed and the mean S_{Hmax} orientation on a regular grid using a search radius of 150 km and a quality and distance weight (Figs. 11 b and c). However, some similarities can be observed. For example, the simple model (Fig. 11 a) shows a clockwise rotation from the NPZ to the MGCH and counter-clockwise from the MGCH to the STZ. The same can be observed less pronounced in the observed S_{Hmax} orientation (Fig. 11 b). The North-North-East S_{Hmax} orientation within the central part of the MGCH is similar between the model, the data and the mean S_{Hmax} orientation (Figs. 11 a-c).

6 Discussion

6.1 Model simplification

This study investigates the influence of elastic material properties, density and the friction coefficient on friction coefficient at vertical faults on the orientation of S_{Hmax} . The focus is not on stress rotation close to the material transition or discontinuity (<10 km), the priority is on the far field effects (>10 km). Although the model may be-is inspired by a particular region, but the goal is to gain a better understanding of the interaction of the on how the variable material properties on-affect the stress orientation (S_{Hmax}). The focus is not on stress rotation close (<5 km) to the material transition or discontinuity, the priority is on the far field effects. Fore sure it. For this reason, the model geometry is very simple and some of the used material properties may have no proper natural equivalent.

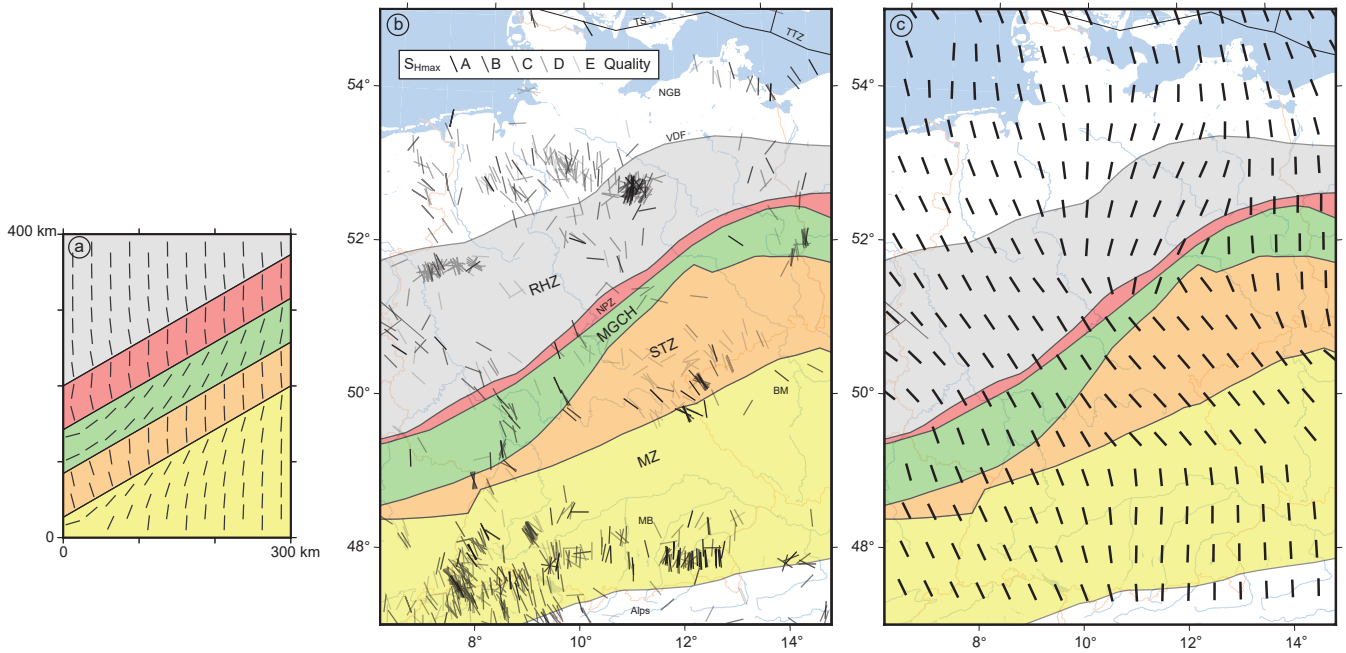


Figure 11. Comparison of orientations of the maximum horizontal stress (S_{Hmax}). The equivalent regions are the RHZ = Rheno-Hercynian Zone, NPZ = Northern Phyllite Zone, the MGCH = Mid-German Crystalline High, the STZ = Saxo-Thuringian Zone and the MZ = Moldanubian Zone a) Model results, application of estimated material properties of the Variscan units (Table 3). Black bars represent the S_{Hmax} orientation at a depth of 1000 m. b) Bars indicate the S_{Hmax} orientation data (Heidbach et al., 2018); quality is indicated by shades of grey, see legend. c) Mean S_{Hmax} orientation on a 150 km search radius with a distance and quality weight ($n > 3$) using the tool stress2grid (Ziegler and Heidbach, 2017). Subfigures b) and c) have the same extent as Fig. 1.

It is really unlikely that ~~such~~ constant materials with such a thickness ~~exists~~ exist somewhere in the crust. ~~Not only the geometry is a strong simplification, but also the neglect of~~ Even within one lithological unit, mechanical properties are not constant with depth, as they increase with depth (Young's modulus, density, etc.) as a result of the acting gravity and compaction, especially for sediments. Each lithological unit is at least partially affected by these changes. Linear increasing rock properties with depth would account for this and be a more realistic representation. But this would not affect the resulting stress pattern. Especially since a vertically uniform stress field is assumed (Zoback et al., 1989; Zoback, 1992; Heidbach et al., 2018), with a few exceptions.

The simple generic models neglect various rheological processes in the crust by applying linear-elastic material ~~laws is a strong simplification~~ law. However, the overall geometry seems reasonable, as the brittle domain or elastic thickness of the ~~crust~~ lithosphere (T_e), which is a measure of the integrated ~~strength~~ stiffness of the lithosphere, is in the order of 30 km and more in central Europe (Tesauro et al., 2012). The Moho depth in ~~Germany or~~ central Europe is also about 30 km ~~(Grad and Tiira, 2009)~~ (Aichroth et al., 1992; Grad and Tiira, 2009). Jarosiński et al. (2006) for example used a range of $T_e =$

30–100 km for their model of central Europe. Furthermore, results are represented and discussed mainly for a depth of 1000 m where elastic behaviour is certainly predominant.

The scenario models were tested with an additional stiff mantle-very stiff mantle (Table 3) with a thickness of 30 km. This had no influence on the observed stress pattern in-at a depth of 1000 mdepth-But- However, the models with the same geometryand
500 ,but a total thickness of only 10 km resulted in much lower stress rotation. Therefore, the elastic thickness of the crust-and-the lithosphere and the aspect ratio of thickness and width of the anomaly-is-an-important-constraint-units are important constraints for the possible stress rotation. The depth at which the stress orientation is plotted is also important, as the stress rotation changes-with-depth-,decreases with depth (Fig. 12), so that it disappears at about 10 km depth for the used configuration. As homogeneous material properties are used, smaller scaling of results seems to be reasonable, considering the aspect ratio.

505 6.2 Boundary conditions

All models were loaded with the same displacement boundary conditions (Fig. 2). This results in slightly different stress magnitudes due to the variable material properties. Since these models have different mechanical properties depending on the unit, the question would arise, in which of the units identical stress magnitudes should be achieved? Even if each model were calibrated individually, this would not significantly change the results, as both the stress regime and stress orientation would
510 remain nearly constant for slightly different boundary conditions. Therefore, constant boundary conditions are reasonable and applied to all scenarios.

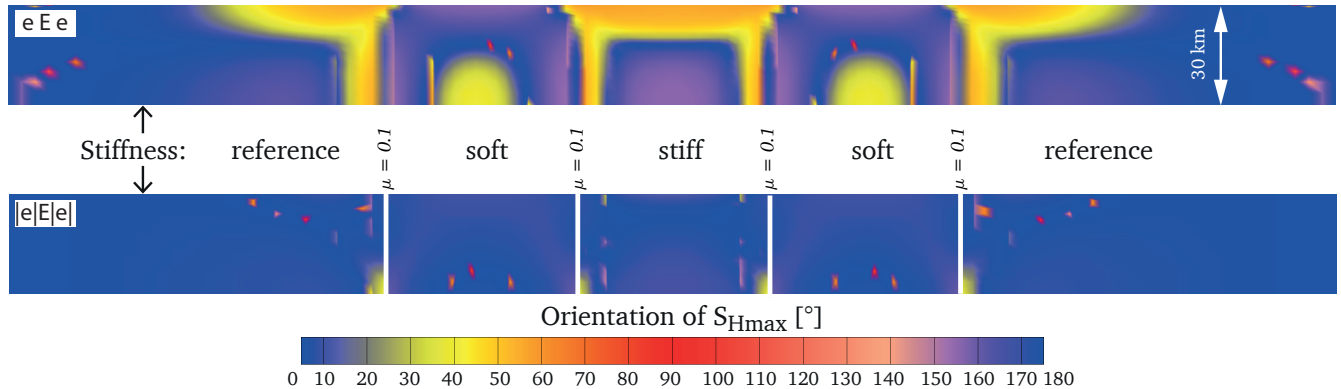


Figure 12. North-south depth profiles displaying the S_{Hmax} orientation colour-coded for models with variable Young's modulus. In the model without the discontinuities (e|e|e), S_{Hmax} is oriented around 40° in the stiffer units next to the softer units near the Earth surface. A similar orientation can be observed in the soft units in the deepest parts. In contrast to that, in the model with the same material properties, but low friction faults (|e|E|e|), the S_{Hmax} orientation is nearly north-south for all units and depths. (Small coloured dots are artefacts.) The discontinuities with a low friction coefficient counterbalances stress rotations by stiffness contrasts.

6.3 Stress rotation by density contrast

The lateral variation of the density is responsible for S_{Hmax} rotation in the range of 7° to 17° (Fig. 6). In general, the S_{Hmax} rotates in the low density units slightly toward parallel to the high density unit ~~+~~ $(+10^\circ)$ whereas S_{Hmax} rotates in the high density units a little bit in the direction to the low density units ~~+~~ (-7°) .

Taking a broad range of sediments into account (~~evaporates~~evaporites, shale, sand- or limestone), they could have even a lower density ~~then~~than the used lowest value ($\rho = 2.2 \text{ g cm}^{-3}$). Most probably, models with a lower stiffness would result in larger stress rotation. However, sediments with a low stiffness could reach a thickness of several thousand meters, but not in the order of the model ~~size~~depth of 30 km or with such a low density due to increasing compaction with depth. Therefore, the impact of density variation on the stress orientation in nature will be much smaller, or on a very local scale. This agrees with the results of Gölke and Coblenz (1996). ~~Observed significant stress rotation are may be a product of other parameters; observation close to the material transition, or low,~~ where a lateral density variation did not have a significant impact on the stress pattern, only local effects are observed.

This assumption seems to be a contradiction to the fact, that the gravitational load is one of the main sources of stress in the Earth's crust. However, a density anomaly is a much smaller influencing variable on the stress state than density. According to Sonder (1990), the resulting stress rotations depend on the relative influence of regional stress sources as opposed to the density anomaly. In case of the model scenarios used, the influence of the boundary conditions (regional stress sources) appears to be greater than that of the density anomaly. Therefore, the model results are probably not representative for regions with small horizontal differential stresses.

6.4 Stress rotation due to a variation of the Poisson's ratio

Model results suggest ~~+~~that the Variation of the Poisson's ratio can be responsible for a S_{Hmax} rotation of ~~about~~up to 7.5° (Fig. 7). This is below the uncertainties of stress orientation estimations of about $\pm 15^\circ$ and more (Heidbach et al., 2018). Therefore, the variation of the Poisson's ratio can be neglected ~~. It was also no literature to detect, investigating that subject. as~~ a potential source of significant stress rotation.

6.5 Stress rotation due to different Young's modulus

The lateral variation of the Young's modulus can lead to significant S_{Hmax} rotation (Fig. 8). For the used geometry and material parameters, the relative ~~rotation~~rotations are up to 78° , which is not far from the maximal possible rotation of 90° . The largest rotation ~~occur in the models~~occurs in the units with the lower Young's modulus, for example the eee model ~~have~~has a total rotation of 78° , whereas the EEE model ~~provides~~causes only 31° rotation. This is not surprising as the Young's modulus is simply a measure of the stiffness. Therefore, largest stress rotation due to stiffness contrast will happen in the soft units, not in the rigid ones. From this, it can be deduced that for units with smaller Young's modulus, the stress rotation is even greater.

S_{Hmax} will be oriented parallel to the structure for stiff units and perpendicular ~~to weak~~for soft units, which agrees with the literature (Bell, 1996; Zhang et al., 1994). The largest stress rotation occurs nearest to the material transition and decreases

with distance to the material transition, similar to other models (Spann et al., 1994). ~~The importance of stiffness differences is an~~
545 ~~result of other models too (Grünthal and Stromeier, 1992; Mantovani et al., 2000; Marotta et al., 2002; Spann et al., 1994; Tommasi et al., 1994).~~
~~Impacts of stiffness contrast have been described in previous studies (Grünthal and Stromeier, 1992; Spann et al., 1994; Tommasi et al., 1994).~~
In contrast to that, Jarosiński et al. (2006) found, that a stiffness contrast has only minor effects. But they did not test the stiffness contrast separately; they applied ~~that it~~ only in combination with active faults in-between the units. However, this agrees with the results of this study, as active faults balance stress rotation by stiffness contrast.

550 ~~Substantial stress rotations are not observed along major Pre-Mesozoic boundaries and sutures in the eastern United States, like the Greenville front, a suture from Missouri to New York, or in the Appalachian Mountains (Zoback, 1992). Gregersen (1992) reports the same from Fennoscandia. In the case that these tectonic boundaries did not provide a significant stiffness transition, it is not a contradiction to this study.~~
~~Within the units having a small Young's Modulus, significant deformation is possible. For example, within the eEe Model (Fig. 8), the soft units in green will be sinistrally deformed. The stiff unit in red cannot be~~
555 ~~deformed in the same way. But as the units are connected, the stiff unit is affected by the tangentially acting stress source. This leads to a S_{Hmax} orientation parallel to the structure, within the stiff units. As the soft one allows such deformation, S_{Hmax} will be oriented normal to the stiff unit.~~

At the interface between stiff and soft units differential stresses are greatest, as both units are differently deformable. This fits with the observation of concentrated intra-plate earthquakes around cratons (Mooney et al., 2012). On a smaller scale this has
560 been observed for stiff sedimentary layers or rigid dykes, which attracts the occurrence of seismicity (Roberts and Schweitzer, 1999; Ziegler et al., 2003).

The observed radial stress pattern ~~southward to the south~~ of the Bohemian massif (Reinecker and Lenhardt, 1999) agrees well with this study, where S_{Hmax} ~~is perpendicular~~ in the soft sediments of the Upper and Lower Austrian basin ~~directed is~~
565 ~~perpendicular~~ to the stiff ~~crystalline crystalline~~ Bohemian Massif. ~~More ambiguous would that be~~ This is more ambiguously
the case for the fan shaped pattern in the western and northern part of the Alpine ~~molasses molasse~~ basin (Grünthal and Stromeier, 1992; Kastrup et al., 2004; Reinecker et al., 2010). As reasons, a lateral stiffness contrast of the rock could play a ~~role~~
role, next to the topographic features of the mountain chain and the overall crustal structure.

~~Furthermore, important is the depth of observed stress rotation. When comparing the stress rotation, it is important to consider the respective depth (see Fig. 12).~~ For example, data in the north-western Alps ~~are dominant originate from~~ focal mechanisms
570 and in the ~~north-eastern Alps foreland of the central Alps~~, the majority of data are from wells, which are more shallow (Reinecker et al., 2010).

Substantial stress rotations are not observed along major Pre-Mesozoic boundaries and sutures in the eastern United States, like the Greenville front, a suture from Missouri to New York, or in the Appalachian Mountains (Zoback, 1992). Gregersen (1992) reports the same for Fennoscandia. In the case that these tectonic boundaries did not provide a significant stiffness transition, it is not
575 a contradiction to this study. The mechanical contrast is important, not the relative ages.

6.6 Comparison of stress rotation due to elastic material properties

The rotation of S_{Hmax} perpendicular (counter-clockwise) to the structure can be observed in material with a lower Young's modulus next to a material transition most clearly, up to -22° . Rotation in the same direction, but with a ~~less~~ lower amount is observed in rocks with a larger density or a smaller Poisson's ratio. Within the units having a ~~larger~~ greater Young's modulus, S_{Hmax} rotates ~~significant~~ significantly parallel (clockwise) to the material transition, up to 56° . Similar rotation with a smaller magnitude can be observed in the low density units or in the units with a larger Poisson's ratio. As rocks with a larger Young's modulus will usually have a larger density and vice versa (Fig. 3), real rocks will have less S_{Hmax} rotation as suggested by ~~this~~ these generic models. But the aim of this study is to test and combine the possible range of variation, in order to identify the most important causes (Fig. 13).

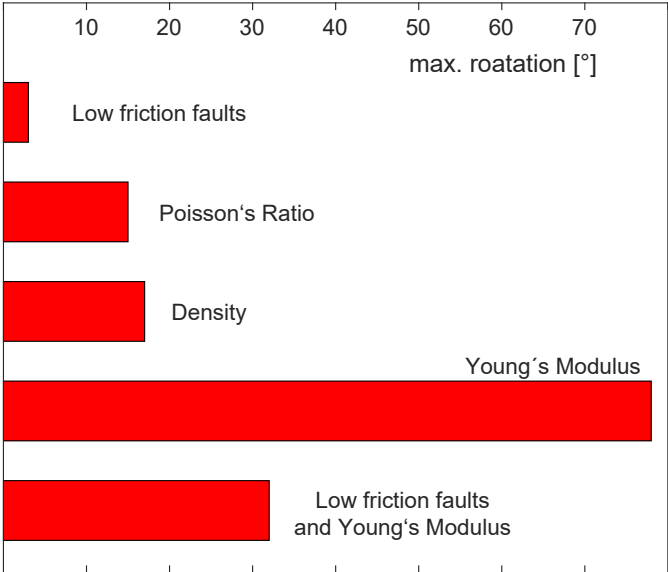


Figure 13. Comparison of resulting maximum stress rotation, based on the used geometry (Fig. 2) and the varied properties (Table 2).

585 6.7 Failure criteria

As only elastic material properties are used, failure is not possible. To study the influence of this simplification, two models (EEE and eee) have been calculated using two different Coulomb failure criteria. The models are run first with a cohesion (C) of 30 MPa and a friction angle (FA) of 40° and in addition with C=10 MPa and a FA of 30°.

590 For the EEE model with C=30 MPa and FA=40°, no failure will be reached (Yield criteria <1). For the eee model using that criteria and for both models (EEE and eee) using C=10 MPa and FA=30° failure occurs. Conditions of failure or close to failure (Yield criteria ~1 or >1) occurs only near the surface (a few km) and close to the material transition (~20-30 km).

Around the material transition, (near) failure can be observed within the stiff units only. For the EEE model with $C=10$ MPa and $FA=30^\circ$, failure is more spaciouly distributed near the surface.

595 In the case of failure, the S_{Hmax} orientation will be balanced, which means, that S_{Hmax} rotates back in the north-south orientation, similar to the applied boundary conditions. In general, failure compensates for stress rotation in the same way as low friction contact surfaces (faults) does. However, the stress orientation in the models that account for failure shows a similar stress pattern in the pre-failure phase as the models without failure. As a conclusion from this observation, the model results showing significant stress rotation are still valid for solid rocks.

6.8 Effect of faults on stress orientation

600 According to the model results, the influence of low friction faults can be neglected concerning the orientation of the far field stress pattern for homogeneous units. The low friction faults ($C=0$, $\mu=0.1$; $FA\ 5^\circ$) lead to only 3° S_{Hmax} rotation ~~in at~~ a distance of about 12.5 km next to the fault zone. Observed stress rotation is lower than 1° for a friction coefficient $\mu>0.4$. This is not in contrast to the strong stress perturbation, observed in the vicinity of faults as one of the three principal stresses must be oriented perpendicular to a fault, the two remaining ones are parallel to the discontinuity (Bell et al., 1992; Bell, 1996; Jaeger et al., 2007). Observations from ~~outerops investigations indicates~~ meso-scale outcrops indicate stress perturbation within 2 km (Petit and Mattauer, 1995) or less than 1 km to a fault (Rispoli, 1981); larger stress perturbation ~~is to observe~~ can be observed at the termination of the fault (2-3 km). If S_{Hmax} is parallel next to the fault, it will rotate by ~~90°~~ 90° at the ~~fault termination~~ (Osokina, 1988; Rispoli, 1981) termination of the fault (Rispoli, 1981; Osokina, 1988).

Yale (2003) suggests significant stress rotation as a product of active faults within a distance of several hundred meters for large differential stress provinces and several kilometres for regions with small differential stresses. This is supported by observed stress rotations near a fault within a range of a few hundred meters to a few kilometres (Brudy et al., 1997; Yassir and Zerwer, 1997). However, not all observed stress rotation agrees to the presented models, like observations offshore eastern Canada (~~Adams and Bell, 1991; Bell and McCallum, 1990~~) (Bell and McCallum, 1990; Adams and Bell, 1991) where stress rotation occur ~~in at~~ a distance of about 10-15 km to a fault. Whether this is due to an inaccurate localization of the fault, a low Young's modulus or other causes cannot be clarified here.

615 Numerical models investigating stress rotations near a fault ~~provides~~ provide stress rotation between 20° and 60° , next to the fault, depending on the fault strike, the boundary conditions and the friction or weakness of the fault. Near the termination of the fault, stress rotation increases to $50-90^\circ$ (~~Homberg et al., 1997; Tommasi et al., 1995; Zhang et al., 1994~~) (Zhang et al., 1994; Tommasi et al., 1995). However, rotation is observed by these models only within 2-3 elements, away from the discontinuity, which are anyway needed to distribute the deformation ~~in by~~ such numerical models. Therefore, observed distances of rotation within these models are not considered here. To avoid this ~~, the orientations~~ influence of a too coarse mesh, the orientation of S_{Hmax} in this study is displayed at least four elements away from the contact surface. ~~In addition, FEM models are unsuitable for representing complex stress-strain patterns near the fault termination if no sufficiently high resolution mesh is available.~~

6.9 Effect of faults combined with stiffness contrasts on stress orientation

625 The models with low friction faults and a variable stiffness (Fig. 10) illustrate much lower stress rotation ~~then~~ than the models without the faults (Fig. 8). The reason is that the soft units cannot transfer tangential shear stresses to the stiffer units. Therefore, each unit can be deformed independently from each other.

It seems to be that discontinuities play an important role to reduce stress ~~rotation~~ rotations, produced by lateral Young's modulus variation. ~~Regarding to~~ (or other reasons). Regarding the used model geometry and materials, the S_{Hmax} variation is
630 reduced for the soft models from 78° to 32° , for a comparison of eee and lelelel in Figs. 8 and 10, using a friction coefficient of $\mu = 0.1$. Also for the mixed models, a ~~change~~ reduction from 78° to 19° is significant. Much lower is the rotation for the ~~stiffer~~ stiff model, with a reduction from 31° to 8° ~~rotation~~ (EEE (EEE in contrast to lElElE)).

The ~~interaction of influence of~~ low friction faults in combination with variable mechanical properties was also investigated for the models with a density contrast. The observed effects are limited; therefore, presentation of the results is omitted.

635 6.10 Depth variation

The interaction of units with a variable Young's modulus and presence or non-presence of low friction faults is visible in Fig. 12. While the model without active faults displays significant stress rotation, the same setting with low friction faults shows only little rotation. The observed stress rotation within the model without faults strongly depends on the depth. In the soft units, S_{Hmax} rotates counter-clockwise near the surface (0 to ~~-8~~ -8 km). In contrast to that a clockwise rotation can be
640 observed ~~in at~~ greater depth (18–30 km).

~~The likelihood of seismicity or faults near the interface between stiff and soft units is larger, since differential stresses are greatest there. This fits with the observation of concentrated intraplate earthquakes around cratons (Mooney et al., 2012). On a smaller scale this has been observed for stiff sedimentary layers or rigid dykes, which attracts the occurrence of seismicity (Roberts and Schweitzer, 1999; Ziegler et al., 2015) The stiffer units show an clockwise rotation in the upper part, about 0 to~~
645 ~~-8 km, which changes slightly to a counter-clockwise orientation in the deeper part.~~

~~North-south depth profiles displaying the S_{Hmax} orientation colour-coded for a models with variable Young's modulus. In the model without the discontinuities (eEe), S_{Hmax} is oriented around 40° in the stiffer units next to the softer units near the Earth surface. A similar orientation can be observed in the soft units in the deepest parts. In contrast to that, in the model with the same material properties, but low friction faults (lelElEl), the S_{Hmax} orientation is nearly north-south for all units and~~
650 ~~depths. (Small coloured dots are artefacts.) The discontinuities with a low friction coefficient counterbalances stress rotations by stiffness contrasts. This could be an indication that stress rotations due to stiffness contrasts in or near sedimentary basins can be significantly greater than in deeper material transitions, such as in a buried crystalline basement. This is all the more likely as sediments tend to be less stiff than crystalline rock.~~

6.11 Comparison of model results with observed stress orientations

6.10.1 Variscan basement in Germany

6.11 Model using the Variscan zone rock properties

Comparison of modelling results with the stress orientation in the German Variscides is only possible to a certain limit, as the model did not reproduce the detailed structural features of the basement structures and certainly not the (partly) overlying sediments. The comparison will concern only [Fig. 11 presents comparatively](#) the results of the models investigating the Young's modulus, as this material parameter have the strongest impact. Taking the structural zonation of the European Variscides of Kossmat (1927) into account, cumulative allocation of geomechanical properties is needed to compare the model results. The Rheno-Hercynian Zone (RHZ) and the Northern Phyllite Zone (NPZ) are dominated by elastic shelf sediments with an low- or mid-metamorphic overprint, which are slate (RHZ) and phyllite (NPZ). This zone, the RHZ and the NPZ together, is the weakest, and will have the lowest Young's modulus. The Mid-German Crystalline High (MGCH) consists of granitoids or gabbros and their metamorphic equivalents (gneiss, amphibolite), meta-sediments and some volcanites. Therefore, this zone is a stiff unit. The Saxo-Thuringian Zone (STZ) is dominated by meta-sediments, mafic and felsic magmatites and their metamorphosed equivalents, and some high-grade metamorphic rocks (granulite, eklogite). Taking all the different rock types into account, the STZ is more stiff as the RHZ and weaker than the MGCH. Mechanical, the Moldanubian zone (MZ) can be represented by high-grade metamorphic rocks (gneiss, granulite, migmatite) and granitoids and will be a stiff unit, similar to the MGCH. Therefore, the units are from the deformable to the rigid ones: $RHZ < STZ < MGCH \approx MZ$. According to the model results (Fig. 8), the S_{Hmax} orientation in the RHZ should deflected counter-clockwise, in the STZ slightly counter-clockwise, and clockwise rotation in the MGCH and MZ.

Material properties used for the Variscan basement units. The properties are estimated based on: Young's Poisson's Vasiscan Density modulus ratio units ρ E ν $g\ cm^{-3}$ MPa Rheno-Hercynian (RHZ) 2.10 20 0.15 N. Phillyite (NPZ) 2.20 30 0.15 Mid-German C. (MGCH) 2.75 70 0.30 Saxo-Thuringian (STZ) 2.60 50 0.25 Moldanubian (MZ) 2.75 70 0.30

To do this, adoption of the model with dimensionally appropriate elastic material properties would be the best option. These material properties are estimated based on typical rock values (Tab. 3 ?). The same initial stress procedure and the same boundary condition and visualization as well is applied. The resulting [orientation of the model using the chosen material properties, inspired by the Variscan units \(a\), the \$S_{Hmax}\$ orientation is visualized in Fig. ?? and will be compared with observed orientation data \(b\) and the averaged orientation of \$S_{Hmax}\$ orientation in Fig. 1.](#)

Application of estimated material properties of the Variscan units (Tab. 3). Black bars represents the orientations of the maximum horizontal stress (S_{Hmax}) at a depth of 1000 m. The equivalent regions are the RHZ = Rheno-Hercynian Zone, NPZ = Northern Phillyite Zone, the MGCH = Mid-German Crystalline High, the STZ = Saxo-Thuringian Zone and the MZ = Moldanubian Zone; compare Fig. 1.

At the transition between the NPZ to the MGCH, a significant clockwise rotation of [on a regular grid \(c\). A limitation of the mean stress orientation on a regular grid \(Fig. 11c\) is the calculation based on distance, and not depending on the specific](#)

unit. The similarity of the S_{Hmax} can be observed within the MGCH (Fig. ??). A much lower but similar stress rotation can be seen at the transition from NPZ to MGCH in Fig. 1 along the river Rhine. Following that line, crossing the border to the STZ displays a counter-clockwise stress rotation, which is also suggested by the model (Fig. ??). Counter-clockwise rotation is also visible at the same unit boundary near the Main river. In general, the orientation is not very convincing, because the overall pattern cannot be reproduced. Some of the deviations from the trend are similar, some are not.

There are probably several reasons, why the simple model is not able to reproduce the observed stress pattern in the German Variscides (Fig. 11). First of all, only a single elastic material composition represent each of the Variscan units. The model did not reproduce the complex and uncertain vertical variability of the deeper structures (Franke et al., 1990; Aichroth et al., 1992; Blundell et al., 1999) as no deep wells are present there. Only refraction seismic profiles from the 1980's (DEKORP) and their interpretations are available (Meissner and Bortfeld, 1990). Consequently, besides the uncertain structures, the material properties and the dip of the unit boundaries are also uncertain.

Of course, it could also be possible that the units are decoupled. Thus, a scenario was calculated, in which the units are separated by low friction faults. But this did not provide a better fit of the stress orientation in the STZ is counter-clockwise rotated to the orientations from the MGCH unit. S_{Hmax} orientation from the Harz (Fig. 1) seems to fit quite well to the model results (Fig. ??). However, structures there are complex and other factors could play an important role. Also taking the counter-clockwise rotation of S_{Hmax} from STZ to the MZ fits with modelling results. But the contrast to the observation. Furthermore, there are no seismic or geodetic indications for such a decoupling of the units in that region.

Structures outside the Variscan zonation may also play a role. To the south, the stress pattern in the molasses basins Molasses Basin is probably more governed by the Alpine orogeny. In general, there are some similarities to observe, but frankly speaking, the model results are not able to prove the significant influence of the material properties on the stress orientation for this region.

Localization of individual grabens and volcanism in the European Cenozoic graben system can be related to late Hereynian fracture systems (?). structure of the Alpine chain (Reinecker et al., 2010) then older structures. The fan shaped stress pattern in the eastern part of the North German Basin has been explained as an effect of the close boundary to the stiff Eastern European Craton along the north-west to south-east striking Teisseyre-Tornquist Zone (TTZ, Goes et al., 2000; Gölke and Coblenz, 1996; Grünthal, 1994; Grünthal and Stromeier, 1986, 1992, 1994; Gölke and Coblenz, 1996; Goes et al., 2000; Kaiser et al., 2005; Marotta et al., 2005). This interpretation agrees well with the results of the models, where S_{Hmax} becomes perpendicular in a soft unit (NGB) directed to a stiff region, like the East European Craton (e.g. model eee in Fig. 8).

Large spatial stress rotations are observed in Australia (Heidbach et al., 2018) and Northern America (Lund-Snee and Zoback, 2018, 2020). The variable basement structures there and consequently variable mechanical properties are good candidates to explain the complex stress pattern.

7 Conclusions

The ~~impact of effect of varying~~ elastic material parameters (Young's modulus and Poisson's ratio), ~~the body force (density) and~~
720 ~~low frietions density and low friction~~ discontinuities on the ~~map-view stress pattern~~ stress pattern in map view is investigated. Each property is tested separately to avoid interdependencies. This is ~~realized~~ performed with generic 3-D models using the finite element method. ~~Within the models, three units with~~ Three units of variable material properties are ~~incorporated,~~
~~where the boundary conditions govern~~ included within the models, with boundary conditions determining the overall S_{Hmax} orientation. The variation of density and the Poisson's ratio lead to small rotation ($\leq 17^\circ$) ~~of the maximum horizontal stress~~
725 ~~(17° and 7.5°) of S_{Hmax}).~~ In contrast ~~to that, a stiffness contrast,~~ stiffness variation is able to produce significant stress rotation of 31° to 78° . Therefore, ~~the~~ variation of the Young's modulus in the upper crust ~~are~~ is a potent explanation for observed stress rotation. Faults are represented in the models by cohesionless contact surfaces. ~~Observed far field stress rotation~~ The
observed stress rotation in the far field due to low friction faults ($\mu = 0.1$) is less ~~as~~ than 3° . Implementation of low friction discontinuities in models with ~~the a~~ Young's modulus anomaly ~~leads to results in~~ much smaller S_{Hmax} rotation, in the order of
730 8° to 32° . ~~Following that, faults did not produce far field~~ It follows that faults do not produce far field stress rotation, ~~they~~
~~rather compensate stress rotation which are effect by~~ but rather compensate for stress rotation that is an effect of the Young's modulus anomaly or other causes. Comparison of the model results with the observed stress orientation in the region ~~, which~~
~~that~~ inspired the models ~~, provides~~ provides only limited consistency. Nevertheless, the studies clearly show that fault systems
are hardly the source of stress rotations on length scale of 100 km or larger. Furthermore, the study indicate that strength
735 contrasts are promising candidates that have the potential to explain the slightly stress pattern rotations in intraplate settings
where topography and low friction fault systems are missing.

Competing interests. The author declare that he has no conflict of interest.

Acknowledgements. I want to thank Oliver Heidbach, Tobias Hergert, Birgit Müller and Moritz Ziegler for fruitful discussions about
mechanics in the upper crust and the observed stress rotation pattern and comments on the manuscript as well. Also I would like to thank
740 two anonymous reviewers for their constructive annotation, which improve the manuscript. Maps and model illustrations were generated using GMT software (Wessel et al., 2013). ~~The author declare that he has no conflict of interest.~~ This study is part of the SpannEnD Project
(www.SpannEnD-Projekt.de) funded by the Federal Ministry for Economic Affairs and Energy (BMWi) and managed by Projektträger
Karlsruhe (PTKA) (project code: 02E11637A).

References

- Adams, J. and Bell, J. S.: Crustal Stresses in Canada, in: *Neotectonics of North America*, chap. 20, pp. 367–386, Geological Society of America, 1991.
- Ahlers, S., Henk, A., Hergert, T., Reiter, K., Müller, B., Röckel, L., Heidbach, O., Morawietz, S., Scheck-Wenderoth, M., and Anikiev, D.: 3D crustal stress state of Western Central Europe according to a data-calibrated geomechanical model – first results, *Solid Earth Discussions*, pp. 1–26, <https://doi.org/10.5194/se-2020-199>, 2020.
- Aichroth, B., Prodehl, C., and Thybo, H.: Crustal structure along the Central Segment of the EGT from seismic-refraction studies, *Tectonophysics*, 207, 43–64, [https://doi.org/10.1016/0040-1951\(92\)90471-H](https://doi.org/10.1016/0040-1951(92)90471-H), 1992.
- Anderson, E. M.: The dynamics of faulting, *Transactions of the Edinburgh Geological Society*, 8, 387–402, <https://doi.org/10.1144/transed.8.3.387>, 1905.
- Anderson, E. M.: *The Dynamics of Faulting and Dyke Formation with Application to Britain*, 2nd ed. Oliver and Boyd, London and Edinburgh, 1951.
- Artyushkov, E. V.: Stresses in the lithosphere caused by crustal thickness inhomogeneities, *Journal of Geophysical Research*, 78, 7675–7708, <https://doi.org/10.1029/JB078i032p07675>, 1973.
- Assameur, D. M. and Mareschal, J.-C.: Stress induced by topography and crustal density heterogeneities: implication for the seismicity of southeastern Canada, *Tectonophysics*, 241, 179–192, [https://doi.org/10.1016/0040-1951\(94\)00202-K](https://doi.org/10.1016/0040-1951(94)00202-K), 1995.
- Bada, G., Cloetingh, S., Gerner, P., and Horvâth, F.: Sources of recent tectonic stress in the Pannonian region: inferences from finite element modelling, *Geophysical Journal International*, 134, 87–101, <https://doi.org/10.1046/j.1365-246x.1998.00545.x>, 1998.
- Bell, J. S.: In situ stresses in sedimentary rocks (part 2): Applications of stress measurements, *Geoscience Canada*, 23, 135–153, 1996.
- Bell, J. S. and Lloyd, P. F.: Modelling of stress refraction in sediments around the Peace River Arch, Western Canada., *Current Research, PartD. Geological Survey of Canada*, 89, 49–54, 1989.
- Bell, J. S. and McCallum, R.: In situ stress in the Peace River Arch area, Western Canada, *Bulletin of Canadian Petroleum Geology*, 38, 270–281, 1990.
- Bell, J. S., Caillet, G., and Adams, J.: Attempts to detect open fractures and non-sealing faults with dipmeter logs, *Geological Society, London, Special Publications*, 65, 211–220, <https://doi.org/10.1144/GSL.SP.1992.065.01.16>, 1992.
- Blundell, D. J., Freeman, R., Müller, S., Button, S., and Mueller, S.: A continent revealed: The European Geotraverse, structure and dynamic evolution, *Cambridge University Press, Cambridge*, <https://doi.org/10.1017/CBO9780511608261>, 1992.
- Bott, M. and Dean, D. S.: Stress Systems at Young Continental Margins, *Nature Physical Science*, 235, 23–25, <https://doi.org/10.1038/physci235023a0>, 1972.
- Brown, E. T. and Hoek, E.: Trends in relationships between measured in-situ stresses and depth, *International Journal of Rock Mechanics and Mining Sciences & Geomechanics Abstracts*, 15, 211–215, [https://doi.org/10.1016/0148-9062\(78\)91227-5](https://doi.org/10.1016/0148-9062(78)91227-5), 1978.
- Brudy, M., Zoback, M. D., Fuchs, K., Rummel, F., and Baumgärtner, J.: Estimation of the complete stress tensor to 8 km depth in the KTB scientific drill holes: Implications for crustal strength, *Journal of Geophysical Research: Solid Earth*, 102, 18453–18475, <https://doi.org/10.1029/96JB02942>, 1997.
- Buchmann, T. J. and Connolly, P. T.: Contemporary kinematics of the Upper Rhine Graben: A 3D finite element approach, *Global and Planetary Change*, 58, 287–309, <https://doi.org/10.1016/j.gloplacha.2007.02.012>, 2007.
- Byerlee, J.: Friction of Rocks, *Pure and Applied Geophysics PAGEOPH*, 116, 615–626, <https://doi.org/10.1007/BF00876528>, 1978.

- Coblentz, D. D. and Richardson, R. M.: Statistical trends in the intraplate stress field, *Journal of Geophysical Research*, 100, 20245, <https://doi.org/10.1029/95JB02160>, 1995.
- Cornet, F. H. and Röckel, T.: Vertical stress profiles and the significance of “stress decoupling”, *Tectonophysics*, 581, 193–205, <https://doi.org/10.1016/j.tecto.2012.01.020>, 2012.
- 785 Di Toro, G., Han, R., Hirose, T., De Paola, N., Nielsen, S., Mizoguchi, K., Ferri, F., Cocco, M., and Shimamoto, T.: Fault lubrication during earthquakes, *Nature*, 471, 494–498, <https://doi.org/10.1038/nature09838>, 2011.
- Eisbacher, G. H. and Bielenstein, H. U.: Elastic strain recovery in Proterozoic rocks near Elliot Lake, Ontario, *Journal of Geophysical Research*, 76, 2012–2021, <https://doi.org/10.1029/JB076i008p02012>, 1971.
- Engelder, T.: Deviatoric stressitis: A virus infecting the Earth science community, *Eos, Transactions American Geophysical Union*, 75, 209, <https://doi.org/10.1029/94EO00885>, 1994.
- 790 Evans, K. F., Engelder, T., and Plumb, R. A.: Appalachian Stress Study: 1. A detailed description of in situ stress variations in Devonian shales of the Appalachian Plateau, *Journal of Geophysical Research*, 94, 7129, <https://doi.org/10.1029/JB094iB06p07129>, 1989.
- Fleitout, L. and Froidevaux, C.: Tectonics and topography for a lithosphere containing density heterogeneities, *Tectonics*, 1, 21–56, <https://doi.org/10.1029/TC001i001p00021>, 1982.
- 795 Fordjor, C. K., Bell, J. S., and Gough, D. I.: Breakouts in Alberta and stress in the North American plate, *Canadian Journal of Earth Sciences*, 20, 1445–1455, <https://doi.org/10.1139/e83-130>, 1983.
- Frank, F. C.: Plate Tectonics, the Analogy with Glacier Flow, and Isostasy, in: *Flow and Fracture of Rocks*, edited by Heard, H. C., Borg, I. Y., Carter, N. L., and Raleigh, C. B., pp. 285–292, AGU, Washington D.C., geophysica edn., <https://doi.org/10.1029/GM016p0285>, 1972.
- 800 Franke, W.: The mid-European segment of the Variscides: tectonostratigraphic units, terrane boundaries and plate tectonic evolution, *Geological Society, London, Special Publications*, 179, 35–61, <https://doi.org/10.1144/GSL.SP.2000.179.01.05>, 2000.
- Franke, W.: The Variscan orogen in Central Europe: construction and collapse, *Geological Society, London, Memoirs*, 32, 333–343, <https://doi.org/10.1144/GSL.MEM.2006.032.01.20>, 2006.
- Franke, W.: Topography of the Variscan orogen in Europe: Failed-not collapsed, *International Journal of Earth Sciences*, 103, 1471–1499, <https://doi.org/10.1007/s00531-014-1014-9>, 2014.
- 805 Franke, W. and Dulce, J.-C.: Back to sender: tectonic accretion and recycling of Baltica-derived Devonian clastic sediments in the Rheno-Hercynian Variscides, *International Journal of Earth Sciences*, 106, 377–386, <https://doi.org/10.1007/s00531-016-1408-y>, 2017.
- Franke, W., Bortfeld, R. K., Brix, M., Drozdowski, G., Dürbaum, H. J., Giese, P., Janoth, W., Jödicke, H., Reichert, C., Scherp, A., Schmoll, J., Thomas, R., Thünker, M., Weber, K., Wiesner, M. G., and Wong, H. K.: Crustal structure of the Rhenish Massif: results of deep seismic reflection lines Dekorp 2-North and 2-North-Q, *Geologische Rundschau*, 79, 523–566, <https://doi.org/10.1007/BF01879201>, 1990.
- 810 Froidevaux, C., Paquin, C., and Souriau, M.: Tectonic stresses in France: In situ measurements with a flat jack, *Journal of Geophysical Research: Solid Earth*, 85, 6342–6346, <https://doi.org/10.1029/JB085iB11p06342>, 1980.
- Ghosh, A., Holt, W. E., Flesch, L. M., and Haines, A. J.: Gravitational potential energy of the Tibetan Plateau and the forces driving the Indian plate, *Geology*, 34, 321–324, <https://doi.org/10.1130/G22071.1>, 2006.
- 815 Ghosh, A., Holt, W. E., and Flesch, L. M.: Contribution of gravitational potential energy differences to the global stress field, *Geophysical Journal International*, 179, 787–812, <https://doi.org/10.1111/j.1365-246X.2009.04326.x>, 2009.
- Goes, S., Loohuis, J., Wortel, M., and Govers, R.: The effect of plate stresses and shallow mantle temperatures on tectonics of northwestern Europe, *Global and Planetary Change*, 27, 23–38, [https://doi.org/10.1016/S0921-8181\(01\)00057-1](https://doi.org/10.1016/S0921-8181(01)00057-1), 2000.

- Gölke, M. and Coblenz, D. D.: Origins of the European regional stress field, *Tectonophysics*, 266, 11–24, [https://doi.org/10.1016/S0040-1951\(96\)00180-1](https://doi.org/10.1016/S0040-1951(96)00180-1), 1996.
- Grad, M. and Tiira, T.: The Moho depth map of the European Plate, *Geophysical Journal International*, 176, 279–292, <https://doi.org/10.1111/j.1365-246X.2008.03919.x>, 2009.
- Grad, M., Polkowski, M., and Ostaficzuk, S. R.: High-resolution 3D seismic model of the crustal and uppermost mantle structure in Poland, *Tectonophysics*, 666, 188–210, <https://doi.org/10.1016/j.tecto.2015.10.022>, 2016.
- Gregersen, S.: Crustal stress regime in Fennoscandia from focal mechanisms, *Journal of Geophysical Research*, 97, 11 821, <https://doi.org/10.1029/91JB02011>, 1992.
- Greiner, G.: In-situ stress measurements in Southwest Germany, *Tectonophysics*, 29, 265–274, [https://doi.org/10.1016/0040-1951\(75\)90150-X](https://doi.org/10.1016/0040-1951(75)90150-X), 1975.
- Greiner, G. and Illies, J. H.: Central Europe: Active or residual tectonic stresses, *Pure and Applied Geophysics*, 115, 11–26, <https://doi.org/10.1007/BF01637094>, 1977.
- Grünthal, G. and Stromeyer, D.: Stress pattern in Central Europe and adjacent areas, *Gerlands Beitr. Geophysik*, 95, 443–452, 1986.
- Grünthal, G. and Stromeyer, D.: The recent crustal stress field in central Europe: Trajectories and finite element modeling, *Journal of Geophysical Research*, 97, 11 805–11 820, <https://doi.org/10.1029/91JB01963>, 1992.
- Grünthal, G. and Stromeyer, D.: The recent crustal stress field in central Europe sensu lato and its quantitative modelling, *Geologie en Mijnbouw*, 73, 173–180, 1994.
- Hast, N.: The state of stresses in the upper part of the earth’s crust: A reply, *Engineering Geology*, 2, 339–344, [https://doi.org/10.1016/0013-7952\(69\)90021-0](https://doi.org/10.1016/0013-7952(69)90021-0), 1969.
- Hast, N.: Global Measurements of Absolute Stress, *Philosophical Transactions of the Royal Society A: Mathematical, Physical and Engineering Sciences*, 274, 409–419, <https://doi.org/10.1098/rsta.1973.0070>, 1973.
- Hast, N.: The state of stress in the upper part of the Earth’s crust as determined by measurements of absolute rock stress, *Die Naturwissenschaften*, 61, 468–475, <https://doi.org/10.1007/BF00622962>, 1974.
- Heidbach, O., Tingay, M. R. P., Barth, A., Reinecker, J., Kurfes, D., and Müller, B.: Global crustal stress pattern based on the World Stress Map database release 2008, *Tectonophysics*, 482, 3–15, <https://doi.org/10.1016/j.tecto.2009.07.023>, 2010.
- Heidbach, O., Rajabi, M., Cui, X., Fuchs, K., Müller, B., Reinecker, J., Reiter, K., Tingay, M. R. P., Wenzel, F., Xie, F., Ziegler, M. O., Zoback, M.-L., and Zoback, M. D.: The World Stress Map database release 2016: Crustal stress pattern across scales, *Tectonophysics*, 744, 484–498, <https://doi.org/10.1016/j.tecto.2018.07.007>, 2018.
- Heim, A.: Untersuchungen über den Mechanismus der Gebirgsbildung im Anschluss an die geologische Monographie der Tödi-Windgällen-Gruppe, Benno Schwabe Verlagsbuchhandlung, Basel, 1878.
- Hergert, T. and Heidbach, O.: Geomechanical model of the Marmara Sea region-II. 3-D contemporary background stress field, *Geophysical Journal International*, 185, 1090–1102, <https://doi.org/10.1111/j.1365-246X.2011.04992.x>, 2011.
- Hergert, T., Heidbach, O., Reiter, K., Giger, S. B., and Marschall, P.: Stress field sensitivity analysis in a sedimentary sequence of the Alpine foreland, northern Switzerland, *Solid Earth*, 6, 533–552, <https://doi.org/10.5194/se-6-533-2015>, 2015.
- Herget, G.: Variation of rock stresses with depth at a Canadian iron mine, *International Journal of Rock Mechanics and Mining Sciences & Geomechanics Abstracts*, 10, 37–51, [https://doi.org/10.1016/0148-9062\(73\)90058-2](https://doi.org/10.1016/0148-9062(73)90058-2), 1973.
- Hickman, S. H. and Zoback, M. D.: Stress orientations and magnitudes in the SAFOD pilot hole, *Geophysical Research Letters*, 31, L15S12, <https://doi.org/10.1029/2004GL020043>, 2004.

- Homberg, C., Hu, J., Angelier, J., Bergerat, F., and Lacombe, O.: Characterization of stress perturbations near major fault zones: insights from 2-D distinct-element numerical modelling and field studies (Jura mountains), *Journal of Structural Geology*, 19, 703–718, [https://doi.org/10.1016/S0191-8141\(96\)00104-6](https://doi.org/10.1016/S0191-8141(96)00104-6), 1997.
- 860 Humphreys, E. D. and Coblenz, D. D.: North American dynamics and western U.S. tectonics, *Reviews of Geophysics*, 45, <https://doi.org/10.1029/2005RG000181>, 2007.
- Jaeger, J. C., Cook, N., and Zimmerman, R.: *Fundamentals of rock mechanics*, Blackwell, 4th edn., 2007.
- Jarosiński, M., Beekman, F., Bada, G., Cloetingh, S., and Jarosinski, M.: Redistribution of recent collision push and ridge push in Central Europe: insights from FEM modelling, *Geophysical Journal International*, 167, 860–880, <https://doi.org/10.1111/j.1365-246X.2006.02979.x>,
865 2006.
- Kaiser, A., Reicherter, K., Hübscher, C., and Gajewski, D.: Variation of the present-day stress field within the North German Basin - Insights from thin shell FE modeling based on residual GPS velocities, *Tectonophysics*, 397, 55–72, <https://doi.org/10.1016/j.tecto.2004.10.009>, 2005.
- Kastrup, U., Zoback, M.-L. L., Deichmann, N., Evans, K. F., Giardini, D., and Michael, A. J.: Stress field variations in the Swiss Alps and the northern Alpine foreland derived from inversion of fault plane solutions, *Journal of Geophysical Research*, 109, B01402, <https://doi.org/10.1029/2003jb002550>, 2004.
870
- King, R., Backé, G., Tingay, M., Hillis, R., and Mildren, S.: Stress deflections around salt diapirs in the Gulf of Mexico, *Geological Society, London, Special Publications*, 367, 141–153, <https://doi.org/10.1144/SP367.10>, 2012.
- Klein, R. and Barr, M.: Regional state of stress in western Europe, in: *Rock stress and rock stress measurement*, pp. 33–44, *International Society for Rock Mechanics and Rock Engineering*, Stockholm, 1986.
875
- Klügel, T., Ahrendt, H., Oncken, O., Käfer, N., Schäfer, F., and Weiss, B.: Alter und Herkunft der Sedimente und des Detritus der nördlichen Phyllit-Zone (Taunussüdrand), *Zeitschrift der Deutschen Geologischen Gesellschaft*, pp. 172–191, 1994.
- Kohlbeck, F., Roch, K.-H., and Scheidegger, A. E.: In Situ Stress Measurements in Austria, in: *Tectonic Stresses in the Alpine-Mediterranean Region*, edited by Scheidegger, A. E., pp. 21–29, Springer Vienna, Vienna, https://doi.org/10.1007/978-3-7091-8588-9_5, 1980.
- 880 Kossmat, F.: Gliederung des varistischen Gebirgsbaues, *Abhandlungen des Sächsischen Geologischen Landesamtes*, 1, 1–39, 1927.
- Kroner, U. and Romer, R. L.: Two plates - Many subduction zones: The Variscan orogeny reconsidered, *Gondwana Research*, 24, 298–329, <https://doi.org/10.1016/j.gr.2013.03.001>, 2013.
- Kroner, U., Hahn, T., Romer, R. L., and Linnemann, U.: The Variscan orogeny in the Saxo-Thuringian zone—heterogenous overprint of Cadomian/Paleozoic peri-Gondwana crust, *Special Paper 423: The Evolution of the Rheic Ocean: From Avalonian-Cadomian Active Margin to Alleghenian-Variscan Collision*, 423, 153–172, [https://doi.org/10.1130/2007.2423\(06\)](https://doi.org/10.1130/2007.2423(06))., 2007.
885
- Laubach, S. E., Clift, S. J., Hill, R. E., and Fix, J.: Stress Directions in Cretaceous Frontier Formation, Green River Basin, Wyoming, in: *Rediscover the Rockies; 43rd Annual Field Conference Guidebook*, pp. 75–86, 1992.
- Lindner, E. N. E. N. and Halpern, J. A.: In-situ stress in North America: A compilation, *International Journal of Rock Mechanics and Mining Sciences & Geomechanics Abstracts*, 15, 183–203, [https://doi.org/10.1016/0148-9062\(78\)91225-1](https://doi.org/10.1016/0148-9062(78)91225-1), 1978.
- 890 Linnemann, U. e.: *Das Saxothuringikum: Abriss der präkambrischen und paläozoischen Geologie von Sachsen und Thüringen*, Staatliche Naturhistorische Sammlung Dresden, Museum für Mineralogie und Geologie, Dresden, geological edn., 2004.
- Lund, B. and Zoback, M. D.: Orientation and magnitude of in situ stress to 6.5 km depth in the Baltic Shield, *International Journal of Rock Mechanics and Mining Sciences*, 36, 169–190, [https://doi.org/10.1016/S0148-9062\(98\)00183-1](https://doi.org/10.1016/S0148-9062(98)00183-1), 1999.

- Lund Snee, J.-E. and Zoback, M. D.: State of stress in the Permian Basin, Texas and New Mexico: Implications for induced seismicity, *The Leading Edge*, 37, 127–134, <https://doi.org/10.1190/tle37020127.1>, 2018.
- Lund Snee, J.-E. and Zoback, M. D.: Multiscale variations of the crustal stress field throughout North America, *Nature Communications*, 11, 1–9, <https://doi.org/10.1038/s41467-020-15841-5>, 2020.
- Mantovani, E., Viti, M., Albarello, D., Tamburelli, C., Babbucci, D., and Cenni, N.: Role of kinematically induced horizontal forces in Mediterranean tectonics: insights from numerical modeling, *Journal of Geodynamics*, 30, 287–320, [https://doi.org/10.1016/S0264-3707\(99\)00067-8](https://doi.org/10.1016/S0264-3707(99)00067-8), 2000.
- Marotta, A. M., Bayer, U., Thybo, H., and Scheck-Wenderoth, M.: Origin of the regional stress in the North German basin: Results from numerical modelling, *Tectonophysics*, 360, 245–264, [https://doi.org/10.1016/S0040-1951\(02\)00358-X](https://doi.org/10.1016/S0040-1951(02)00358-X), 2002.
- Martínez-Garzón, P., Bohnhoff, M., Kwiatak, G., and Dresen, G.: Stress tensor changes related to fluid injection at The Geysers geothermal field, California, *Geophysical Research Letters*, 40, 2596–2601, <https://doi.org/10.1002/grl.50438>, 2013.
- Matte, P.: Tectonics and plate tectonics model for the Variscan belt of Europe, *Tectonophysics*, 126, [https://doi.org/10.1016/0040-1951\(86\)90237-4](https://doi.org/10.1016/0040-1951(86)90237-4), 1986.
- Mazzotti, S. and Townend, J.: State of stress in central and eastern North American seismic zones, *Lithosphere*, 2, 76–83, <https://doi.org/10.1130/L65.1>, 2010.
- McCutchen, W. R.: Some elements of a theory for In-situ stress, *International Journal of Rock Mechanics and Mining Sciences & Geomechanics Abstracts*, 19, 201–203, [https://doi.org/10.1016/0148-9062\(82\)90890-7](https://doi.org/10.1016/0148-9062(82)90890-7), 1982.
- Meissner, R. and Bortfeld, R. K.: DEKORP-Atlas : Results of Deutsches Kontinentales Reflexionsseismisches Programm, Springer, 1990.
- Miller, D. J. and Dunne, T.: Topographic perturbations of regional stresses and consequent bedrock fracturing, *Journal of Geophysical Research: Solid Earth*, 101, 25 523–25 536, <https://doi.org/10.1029/96JB02531>, 1996.
- Minster, J. B. and Jordan, T. H.: Present-day plate motions, *Journal of Geophysical Research*, 83, 5331, <https://doi.org/10.1029/JB083iB11p05331>, 1978.
- Mooney, W. D., Ritsema, J., and Hwang, Y. K.: Crustal seismicity and the earthquake catalog maximum moment magnitude (M_{\max}) in stable continental regions (SCRs): Correlation with the seismic velocity of the lithosphere, *Earth and Planetary Science Letters*, 357–358, 78–83, <https://doi.org/10.1016/j.epsl.2012.08.032>, 2012.
- Müller, B., Zoback, M.-L., Fuchs, K., Mastin, L., Gregersen, S., Pavoni, N., Stephansson, O., and Ljunggren, C.: Regional patterns of tectonic stress in Europe, *Journal of Geophysical Research*, 97, 11 783, <https://doi.org/10.1029/91JB01096>, 1992.
- Müller, B., Heidbach, O., Negut, M., Sperner, B., and Buchmann, T. J.: Tectonophysics Attached or not attached — evidence from crustal stress observations for a weak coupling of the Vrancea slab in Romania, *Tectonophysics*, 482, 139–149, <https://doi.org/10.1016/j.tecto.2009.08.022>, 2010.
- Müller, B., Schilling, F., Röckel, T., and Heidbach, O.: Induced Seismicity in Reservoirs : Stress Makes the Difference, *Erdöl Erdgas Kohle*, 134, 33–37, <https://doi.org/10.19225/180106>, 2018.
- Naliboff, J. B., Lithgow-Bertelloni, C., Ruff, L. J., and de Koker, N.: The effects of lithospheric thickness and density structure on Earth’s stress field, *Geophysical Journal International*, 188, 1–17, <https://doi.org/10.1111/j.1365-246X.2011.05248.x>, 2012.
- Oncken, O.: Transformation of a magmatic arc and an orogenic root during oblique collision and its consequences for the evolution of the European Variscides (Mid-German Crystalline Rise), *Geologische Rundschau*, 86, 2–20, <https://doi.org/10.1007/s005310050118>, 1997.

- 930 Oncken, O., Franzke, H. J., Dittmar, U., and Klügel, T.: Rhenohercynian foldbelt: Metamorphic Units (Northern Phyllite Zone), Structure, in: Pre-Permian Geology of Central and Western Europe, edited by Dallmeyer, R. D., Franke, W., and Weber, K., pp. 109–117, Springer, Berlin, 1995.
- Osokina, D.: Hierarchical properties of a stress field and its relation to fault displacements, *Journal of Geodynamics*, 10, 331–344, [https://doi.org/10.1016/0264-3707\(88\)90039-7](https://doi.org/10.1016/0264-3707(88)90039-7), 1988.
- 935 Petit, J. P. and Mattauer, M.: Palaeostress superimposition deduced from mesoscale structures in limestone: the Matelles exposure, Languedoc, France, *Journal of Structural Geology*, 17, 245–256, [https://doi.org/10.1016/0191-8141\(94\)E0039-2](https://doi.org/10.1016/0191-8141(94)E0039-2), 1995.
- Pierdominici, S. and Heidbach, O.: Stress field of Italy — Mean stress orientation at different depths and wave-length of the stress pattern, *Tectonophysics*, 532–535, 301–311, <https://doi.org/10.1016/j.tecto.2012.02.018>, 2012.
- Plumb, R. A. and Cox, J. W.: Stress directions in eastern North America determined to 4.5 km from borehole elongation measurements, *Journal of Geophysical Research*, 92, 4805, <https://doi.org/10.1029/JB092iB06p04805>, 1987.
- 940 Ranalli, G. and Chandler, T. E.: The Stress Field in the Upper Crust as Determined from In Situ Measurements, *Geologische Rundschau*, 64, 653–674, <https://doi.org/10.1007/BF01820688>, 1975.
- Reinecker, J. and Lenhardt, W. A.: Present-day stress field and deformation in eastern Austria, *International Journal of Earth Sciences*, 88, 532–550, <https://doi.org/10.1007/s005310050283>, 1999.
- 945 Reinecker, J., Tingay, M. R. P., Müller, B., and Heidbach, O.: Present-day stress orientation in the Molasse Basin, *Tectonophysics*, 482, 129–138, <https://doi.org/10.1016/j.tecto.2009.07.021>, 2010.
- Reiter, K. and Heidbach, O.: 3-D geomechanical-numerical model of the contemporary crustal stress state in the Alberta Basin (Canada), *Solid Earth*, 5, 1123–1149, <https://doi.org/10.5194/se-5-1123-2014>, 2014.
- Reiter, K., Heidbach, O., Reinecker, J., Müller, B., and Röckel, T.: Spannungskarte Deutschland 2015, *Erdöl Erdgas Kohle*, 131, 437–442, <https://doi.org/10.1029/98EO00426>, 2015.
- 950 Richardson, R. M., Solomon, S. C., and Sleep, N. H.: Tectonic stress in the plates, *Reviews of Geophysics*, 17, 981–1019, <https://doi.org/10.1029/RG017i005p00981>, 1979.
- Rispoli, R.: Stress fields about strike-slip faults inferred from stylolites and tension gashes, *Tectonophysics*, 75, T29–T36, [https://doi.org/10.1016/0040-1951\(81\)90274-2](https://doi.org/10.1016/0040-1951(81)90274-2), 1981.
- 955 Roberts, M. and Schweitzer, J.: Geotechnical areas associated with the Ventersdorp Contact Reef, Witwatersrand Basin, South Africa, *Journal of the South African Institute of Mining and Metallurgy*, 99, 157–166, 1999.
- Röckel, T. and Lempp, C.: Der Spannungszustand im Norddeutschen Becken, *Erdöl Erdgas Kohle*, 119, 73–80, 2003.
- Roth, F. and Fleckenstein, P.: Stress orientations found in North-East Germany differ from the West European trend, *Terra Nova*, 13, 289–296, <https://doi.org/10.1046/j.1365-3121.2001.00357.x>, 2001.
- 960 Saucier, F., Humphreys, E. D., and Weldon, R.: Stress near geometrically complex strike-slip faults: Application to the San Andreas Fault at Cajon Pass, southern California, *Journal of Geophysical Research*, 97, 5081–5094, <https://doi.org/10.1029/91JB02644>, 1992.
- Schoenball, M. and Davatzes, N. C.: Quantifying the heterogeneity of the tectonic stress field using borehole data, *Journal of Geophysical Research: Solid Earth*, 122, 6737–6756, <https://doi.org/10.1002/2017JB014370>, 2017.
- Sheorey, P. R.: A theory for In Situ stresses in isotropic and transverse isotropic rock, *International Journal of Rock Mechanics and Mining Sciences & Geomechanics Abstracts*, 31, 23–34, [https://doi.org/10.1016/0148-9062\(94\)92312-4](https://doi.org/10.1016/0148-9062(94)92312-4), 1994.
- 965 Sonder, L. J.: Effects of density contrasts on the orientation of stresses in the lithosphere: Relation to principal stress directions in the Transverse Ranges, California, *Tectonics*, 9, 761–771, <https://doi.org/10.1029/TC009i004p00761>, 1990.

- Spann, H., Müller, B., and Fuchs, K.: Interpretation of anomalies in observed stress data at the central graben (north sea) — numerical and analytical approach, *Soil Dynamics and Earthquake Engineering*, 13, 1–11, [https://doi.org/10.1016/0267-7261\(94\)90036-1](https://doi.org/10.1016/0267-7261(94)90036-1), 1994.
- 970 Sperner, B., Müller, B., Heidbach, O., Delvaux, D., Reinecker, J., and Fuchs, K.: Tectonic stress in the Earth's crust: advances in the World Stress Map project, *Geological Society Special Publication*, 212, 101–116, 2003.
- Stein, S., Cloetingh, S., Sleep, N. H., and Wortel, R.: Passive Margin Earthquakes, Stresses and Rheology, in: *Earthquakes at North-Atlantic Passive Margins: Neotectonics and Postglacial Rebound*, pp. 231–259, Springer Netherlands, Dordrecht, https://doi.org/10.1007/978-94-009-2311-9_14, 1989.
- 975 Tesauro, M., Kaban, M. K., and Cloetingh, S. A.: Global strength and elastic thickness of the lithosphere, *Global and Planetary Change*, 90–91, 51–57, <https://doi.org/10.1016/j.gloplacha.2011.12.003>, 2012.
- Tingay, M. R. P., Müller, B., Reinecker, J., Heidbach, O., Wenzel, F., and Fleckenstein, P.: Understanding tectonic stress in the oil patch: The World Stress Map Project, *The Leading Edge*, 24, 1276–1282, <https://doi.org/10.1190/1.2149653>, 2005.
- Tommasi, A., Vauchez, A., and Daudré, B.: Initiation and propagation of shear zones in a heterogeneous continental lithosphere, *Journal of Geophysical Research: Solid Earth*, 100, 22 083–22 101, <https://doi.org/10.1029/95JB02042>, 1995.
- 980 Tullis, T. E.: Reflections on Measurement of Residual-Stress in Rock, *Pure and Applied Geophysics*, 115, 57–68, <https://doi.org/10.1007/bf01637097>, 1977.
- Turcotte, D. L., Schubert, and Schubert, G.: *Geodynamics*, Cambridge University Press, 2014.
- van Wees, J. D., Orlic, B., van Eijs, R., Zijl, W., Jongerius, P., Schreppers, G. J., Hendriks, M., and Cornu, T.: Integrated 3D geomechanical modelling for deep subsurface deformation: a case study of tectonic and human-induced deformation in the eastern Netherlands, *Geological Society Special Publication*, 212, 313–328, <https://doi.org/10.1144/GSL.SP.2003.212.01.21>, 2003.
- 985 Wessel, P., Smith, W. H. F., Scharroo, R., Luis, J., and Wobbe, F.: Generic mapping tools: Improved version released, *Eos, Transactions American Geophysical Union*, 94, 409–410, <https://doi.org/10.1002/2013EO450001>, 2013.
- Yale, D. P.: Fault and stress magnitude controls on variations in the orientation of in situ stress, *Geological Society Special Publication*, 209, 55–64, <https://doi.org/10.1144/GSL.SP.2003.209.01.06>, 2003.
- 990 Yassir, N. A. and Zerwer, A.: Stress regimes in the Gulf coast, offshore Louisiana: Data from well-bore breakout analysis, *AAPG Bulletin*, 81, 293–307, <https://doi.org/10.1306/522B4311-1727-11D7-8645000102C1865D>, 1997.
- Zakharova, N. V. and Goldberg, D. S.: In situ stress analysis in the northern Newark Basin: implications for induced seismicity from CO₂ injection, *Journal of Geophysical Research: Solid Earth*, 119, 1–13, <https://doi.org/10.1002/2013JB010492>.Received, 2014.
- 995 Zhang, Y.-Z., Dusseault, M. B., and Yassir, N. A.: Effects of rock anisotropy and heterogeneity on stress distributions at selected sites in North America, *Engineering Geology*, 37, 181–197, [https://doi.org/10.1016/0013-7952\(94\)90055-8](https://doi.org/10.1016/0013-7952(94)90055-8), 1994.
- Ziegler, M. and Heidbach, O.: Matlab script Stress2Grid, <https://doi.org/10.5880/WSM.2019.002>, 2017.
- Ziegler, M. O., Reiter, K., Heidbach, O., Zang, A., Kwiatek, G., Stromeyer, D., Dahm, T., Dresen, G., Hofmann, G., Stromeyer, D., Dahm, T., Dresen, G., and Hofmann, G.: Mining-Induced Stress Transfer and Its Relation to a $M_{\text{w}} > 1.9$ Seismic Event in an Ultra-deep South African Gold Mine, *Pure and Applied Geophysics*, 172, 2557–2570, <https://doi.org/10.1007/s00024-015-1033-x>, 2015.
- 1000 Ziegler, M. O., Heidbach, O., Zang, A., Martínez-Garzón, P., and Bohnhoff, M.: Estimation of the differential stress from the stress rotation angle in low permeable rock, *Geophysical Research Letters*, 44, 6761–6770, <https://doi.org/10.1002/2017GL073598>, 2017.
- Zoback, M.-L. L.: First- and second-order patterns of stress in the lithosphere: The World Stress Map Project, *Journal of Geophysical Research*, 97, 11 703–11 728, <https://doi.org/10.1029/92JB00132>, 1992.

1005 Zoback, M.-L. L. M. D., Adams, J., Assumpção, M., Bell, J. S., Bergman, E. A., Blümling, P., Brereton, N. R., Denham, D., Ding, J., Fuchs, K., Gay, N., Gregersen, S., Gupta, H. K., Gvishiani, A., Jacob, K., Klein, R., Knoll, P., Magee, M., Mercier, J. L., Müller, B., Paquin, C., Rajendran, K., Stephansson, O., Suarez, G., Suter, M., Udias, A., Xu, Z. H., and Zhizhin, M.: Global patterns of tectonic stress, *Nature*, 341, 291–298, <https://doi.org/10.1038/341291a0>, 1989.